

RESEARCH ARTICLE

Development of a Dynamic Hitch Lift Controller using a Hybrid Control Strategy in A Heavy Combination Vehicle

M. Z. Abdul Manaf^{1,2,*}, S. A. A. Bakar¹, K. Hudha³, and P. M. Samin¹

¹Faculty of Mechanical Engineering, Universiti Teknologi Malaysia, 81300 Johor, Malaysia

²Faculty of Mechanical Technology and Engineering, Universiti Teknikal Malaysia Melaka, 76100 Melaka, Malaysia

³Faculty of Engineering, Universiti Pertahanan Nasional Malaysia, 57000 Kuala Lumpur, Malaysia

ABSTRACT – This study presents a novel hybrid control strategy for the active hitch system, named the Dynamic Hitch Lift (DHIL), comprising a hybrid controller and a force actuator. The controller was designed to mitigate longitudinal load transfer in heavy combination vehicles by reducing the semitrailer pitch rate and rejecting the pitch moment, assisted by the virtual Skyhook moment. The new controller can calculate the desired force of the DHIL actuator to counter incoming load transfer during harsh braking exceeding 0.5 g braking deceleration. The proposed controller was assessed using a verified 12-degrees-of-freedom tractor-semitrailer model in harsh braking tests across different vehicle configurations. The first evaluation involved a stability test to demonstrate the stability of the controller in reducing load transfer across different vehicle configurations. The second evaluation was on controller performance, which revealed that the dynamic vehicle response has efficiently reduced load transfer by up to 9.14%. The third evaluation has focused on the DHIL actuator performance, which indicated that the actuator generated a force of 159,197 N, which translated into a stepper motor torque of 1,695 Nm at a speed of 1,000 rpm. Simulation results affirmed that the proposed DHIL controller was stable and could effectively reduce longitudinal load transfer in heavy combination vehicles during harsh braking.

ARTICLE HISTORY

Received : 22nd July 2023

Revised : 08th Nov. 2023

Accepted : 14th Dec. 2023

Published : 20th Mar. 2024

KEYWORDS

Tractor-semitrailer

Longitudinal load transfer

Pitch rate reduction

Pitch moment rejection

Skyhook moment

Active hitch system

1.0 INTRODUCTION

Harsh longitudinal braking can shift the vehicle's center of gravity towards the direction of motion, which could induce load transfer from the rear to the front tires [1] - [4]. This situation could lead to an unwanted pitching moment that can cause the vehicle to dive forward and subsequently, compromise its stability, handling, and control, and potentially resulting in an accident [5]. The impact is more pronounced in heavy combination vehicles due to their substantial weight. Harsh braking intensifies load transfer on the hitch, creating additional pitch moments [6]. This extra load on the hitch joint imposes additional stress on the tractor's rear axle system which can affect the vehicle's stability. To mitigate the load transfer issue, an energy-absorbing system at the hitch joint is proposed in this study. However, the fixed design of conventional hitch systems has prevented it from suppressing the energy from the load transfer.

To address this issue, this research proposes a novel active hitch system, known as the Dynamic Hitch Lift (DHIL) actuator system. This system has been designed to reduce load transfer by minimizing the pitch moment. The DHIL can accomplish this by generating a counter-vertical force at the hitch joint, which in turn creates an opposing pitch moment. As a result, the DHIL system can dynamically adjust the height of the hitch table. This innovative DHIL actuator system can replace the traditional fifth-wheel device on the tractor chassis, as illustrated in Figure 1. However, it is important to note that this study has exclusively focused on developing a new hybrid control strategy for the DHIL system to mitigate longitudinal load transfer and it has not delved into the intricate workings of the DHIL actuator itself.

Moreover, the developed algorithm employed a software-in-the-loop (SIL) methodology, which utilized a verified vehicle simulation model as the controller plant. The proposed hybrid control strategy aimed to minimize load transfer through a two-step process. Initially, it would mitigate the pitch rate of the semitrailer by treating it as a disruptive factor. Subsequently, the pitch moment rejection strategy, as aided by the Skyhook moment, would further diminish the load transfer. The active system was designed to detect braking events characterized by decelerations exceeding 0.5 g and to trigger the Dynamic Hitch Lift (DHIL) system, which would generate a counter-vertical force at the hitch joint. This action could reduce the load transfer and stabilize the semitrailer's pitch angle. The benefits of minimizing the load transfer may encompass improved braking performance and increased cargo hauling capacity.

Conventional hitch systems allow for a slight pitch angle ($< 12^\circ$) and a big yaw angle for turning [7]. The nature of the hitch system is to connect two units; hence, only a rotational degree of freedom is allowed. Previous research found that the translational motion was insignificant because it did not affect the vehicle's stability in everyday driving. However, later researchers found that the hitch point was where the load was being transferred back and forth in their internal force system [8] - [11]. A small degree of pitch angle was insufficient to counter the load transfer and stabilize the vehicle during harsh braking. Many researchers have proposed a system to allow the hitch to have a vertical translation;

hence, allowing a higher pitch angle free play [9] - [15]. Furthermore, the pitch rate was a disturbance parameter related to the load transfer. A higher pitch rate could occur during harsh braking. Hence, many researchers proposed a disturbance rejection control strategy to reject this type of disturbance [16] - [20]. To ensure the stability of the vehicle, previous researchers have added a new control element, namely, the pitch moment rejection, which would reject the moment occurring at the pitch center of the semitrailer [1], [2], [21]. Lastly, a virtual Skyhook moment was added to the controller to assist in rejecting the unwanted pitch moment and to ensure the stability of the controller [22] - [26].

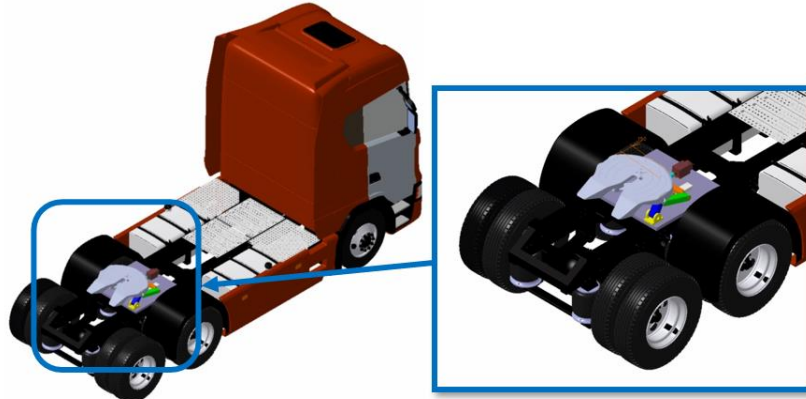


Figure 1. DHIL installation on the tractor chassis

This study has evaluated the proposed control strategy of using the software-in-the-loop-simulation method with the validated 12-DOF tractor-semitrailer longitudinal model by Abdul Manaf et al. [9] based on harsh braking tests. The braking signal from the driver acted as an input into the harsh braking test. MATLAB Simulink software simulated the braking test with different initial braking speeds, semitrailer load conditions, and semitrailer wheelbases. The DHIL control strategy performance was analyzed based on the dynamic and actuator responses of the vehicle. This paper consists of five sections, with the first section presenting an introduction and a review of relevant preliminary works. The second section presents the control strategy of the DHIL using pitch moment rejection with Skyhook assist. Then, the third section discusses the controller stability of the DHIL in terms of initial braking speeds, load conditions, and semitrailer size. Next, the fourth section discusses the DHIL controller performance based on the braking test. Finally, the last section of this paper presents the conclusion of this study.

2.0 DHIL CONTROL STRATEGY

The DHIL controller uses a hybrid control strategy to stabilize the vehicle and reject the unwanted longitudinal load transfer. Therefore, the proposed hybrid control strategy combined the pitch rate reduction (PR) with the pitch moment rejection (PMR), as assisted by the Skyhook moment (Sky). Then, the controller used the semitrailer pitch rate and longitudinal acceleration as controller inputs. Figure 2 depicts the four loops that make up the controller. The validated tractor-semitrailer simulated model served as the plant for generating real signals for this study. These signals originated from the simulated vehicle model in a software-in-the-loop approach. The controller was able to utilize these signals to mitigate pitch moment and reduce load transfer. The novelty of this study was the new hybrid controller, which was applied to the active hitch system located at the hitch joint to reduce the load transfer through pitch moment rejection. The controller would combine the pitch rate reduction and pitch moment rejection, assisted by the Skyhook moment.

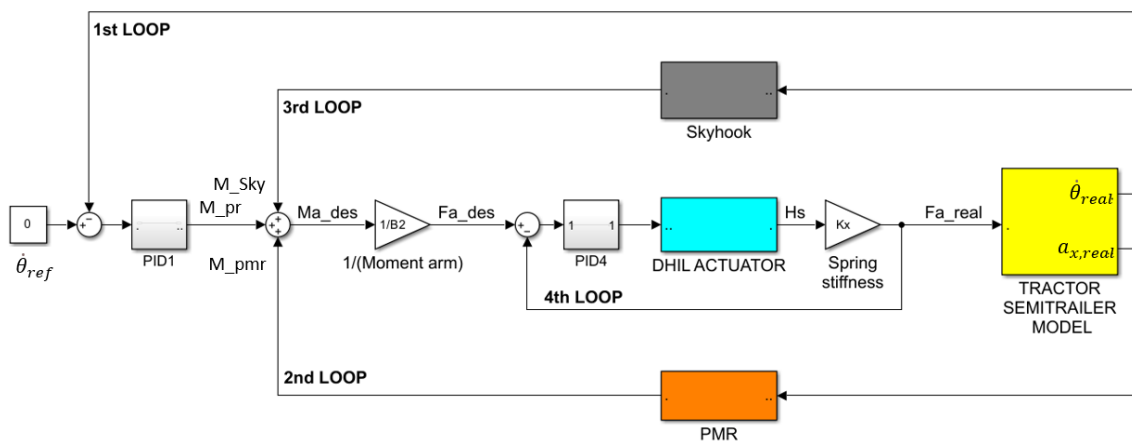


Figure 2. The control strategy of the DHIL

Based on the figure, the first loop controller would use the pitch rate reduction system to stabilize the semitrailer pitch rate. Then, PID1 would tune the pitch rate error and convert the value into the pitch rate moment, M_{pr} . The second loop controller would use the pitch moment rejection system to reduce the longitudinal load transfer by producing the pitch moment, M_{pmr} . The third loop controller would use the Skyhook moment, M_{Sky} , to assist the first and second loop controllers in reducing the load transfer further. Then, the combination of the first, second, and third loops would produce the desired actuator moment, $M_{a,des}$. The desired actuator moment would be converted into the desired actuator force, $F_{a,des}$ before entering the DHIL actuator loop (fourth loop). The fourth loop is the force-tracking control of the DHIL actuator. The DHIL actuator would convert the desired actuator force data into the vertical displacement of the hitch table. This system uses the spring system to measure the real actuator force. The real actuator force, $F_{a,real}$, would be feedforward to the tractor-semitrailer model. Finally, PID4 would tune the desired actuator force as input for the DHIL actuator module.

2.1 Pitch rate reduction system

In the disturbance rejection controller, the system would use the primary parameter rates of change as a disturbance [19], [27] - [31]. One of the control strategies in DHIL was to reject the pitch rate disturbance. The controller would use pitch rate reduction to stabilize the trailer's pitch angle. The pitch rate reference, $\dot{\theta}_{ref}$, would then be compensated by the actual pitch rate, $\dot{\theta}_{real}$, thus, producing an error, $e_1(t)$. This error can be calculated as follows: $e_1(t) = \dot{\theta}_{ref} - \dot{\theta}_{real}$. Next, PID1 would tune the error to produce the pitch moment of the semitrailer, as shown in Equation (1).

$$M_{a,pr} = K_{p1}(t)e_1(t) + K_{i1}(t) \int e_1(t)dt + K_{d1}(t) \frac{d}{dt} e_1(t) \quad (1)$$

2.2 Pitch moment rejection with Skyhook control strategy

In conventional vehicles, the braking force would cause the body's center of gravity to shift forward, which would generate the load transfer from the rear axle to the hitch joint [2], [32]. This phenomenon will generate the pitch moment at the pitch center, M_{pc} , during braking as a response to load transfer. The pitching moment in a conventional vehicle is as shown in Equation (2). Note that the first and second terms are the longitudinal moment of the tractor and semitrailer, respectively. The third and last terms are the longitudinal load transfer moment of the tractor and semitrailer, respectively.

$$M_{pc} = [m_1 a_x](d - H_2 - H_1) + [m_2 a_x]d - \left[\frac{m_1 H K_1}{(B_1 + C_1)} a_x \right] (d - H_2 - H_1) - \left[\frac{m_2 (H_2 - H_1) K_2 B_2}{(B_2 + C_2)} a_x \right] d \quad (2)$$

The harsh braking detection would activate the system in an active DHIL vehicle, as shown in Figure 3. Then, the DHIL actuator force, F_a , would create a counter moment with a similar magnitude to cancel the pitching moment; hence, $M_{a,pmr} = M_{pc}$. Skyhook moment, M_{Sky} , was introduced to virtually assist the DHIL moment to create the moment balance equation. The Skyhook method has been used by many researchers [22] - [25], [33], [34] to stabilize similar vehicles. The application of the Skyhook moment in this study was to act as an extension to the classical Skyhook, which would mainly be used in a vehicle suspension system. The Skyhook moment would act as a virtual damper to reduce the pitching velocity and pitching moment of the semitrailer. Skyhook control can be implemented in two ways, namely, continuous and discontinuous [34] - [36]. In this study, the continuous Skyhook was applied since the controller needed to make continuous corrections to the pitching moment of the vehicle to reduce the load transfer.

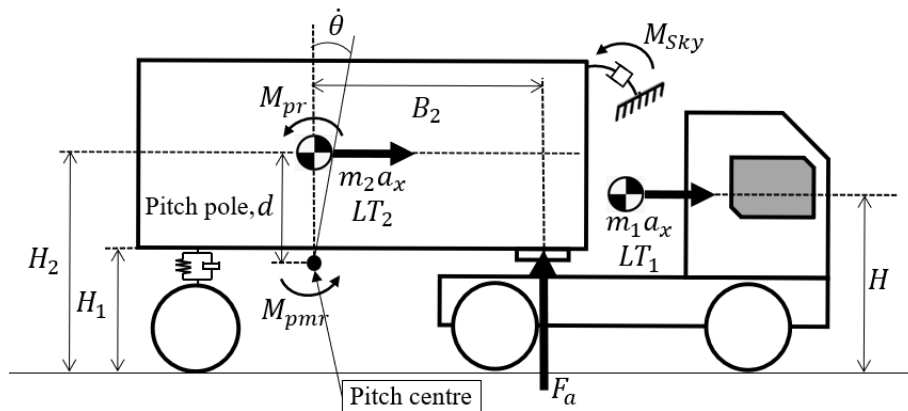


Figure 3. The sum of forces and moments acting on the tractor-semitrailer

Therefore, the desired actuator moment, $M_{a,des}$, is the summation of the pitch rate reduction moment, pitch moment rejection, and Skyhook moment, as shown in Equation (3). The desired actuator force, $F_{a,des}$, can be calculated by dividing $M_{a,des}$, with the moment arm, B_2 , to obtain Equation (4), which is the DHIL controller governing equation. The DHIL

actuator force, $F_{a,des}$, would generate an upward force to absorb the load transfer energy by reducing the semitrailer pitch rate and rejecting the pitch moment that would receive virtual assistance from the Skyhook moment.

$$M_{a,des} = M_{pr} + M_{pmr} + M_{sky} \tag{3}$$

$$F_{a,des} = \frac{1}{B_2} \left\{ \begin{array}{l} K_{p1}(t)e_1(t) + \\ K_{i1}(t) \int e_1(t)dt + \\ K_{d1}(t) \frac{d}{dt} e_1(t) \end{array} \right\} + \left\{ \begin{array}{l} [m_1 a_x](d - H_2 - H_1) + \\ [m_2 a_x]d - \\ \left[\frac{m_1 H K_1}{(B_1 + C_1)} a_x \right] (d - H_2 - H_1) - \\ \left[\frac{m_2 (H_2 - H_1) K_2 B_2}{(B_2 + C_2)} a_x \right] d \end{array} \right\} + \left\{ \frac{1}{d \cdot B_2} C_{sky} \right\} \dot{\theta}_{real} \tag{4}$$

2.3 DHIL actuator model

The DHIL actuator comprises a power screw and a lifting mechanism, as depicted in Figure 4. The power screw is responsible for raising the lifting mechanism to generate the necessary counterforce. This counterforce plays a crucial role in rejecting incoming load transfer and preventing the semitrailer from nose-diving during harsh braking maneuvers. The development of the actuator model hinged on two key parameters, namely, the sizing of the power-screw motor and the maximum lifting height of the lifting mechanism. The determination of these parameters was based on braking test data collected by Abdul Manaf et al. [9]. These tests involved four different vehicle configurations, encompassing 20-foot and 40-foot semitrailers with two load conditions, which were half-laden and full-laden.

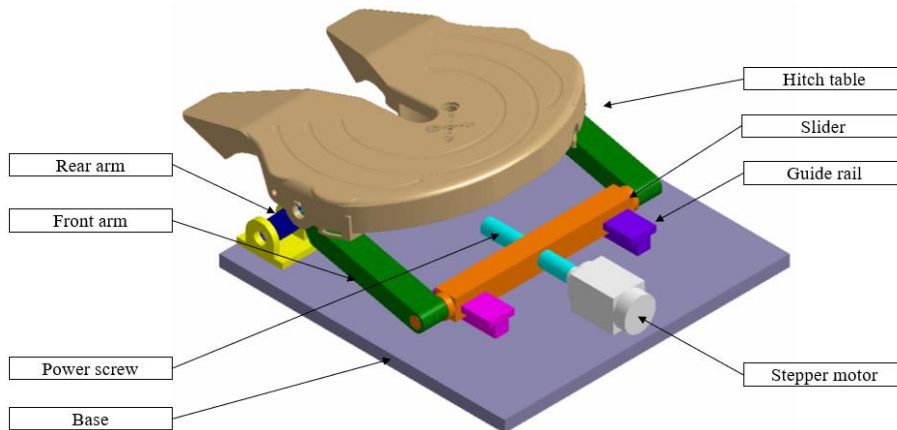


Figure 4. DHIL actuator components and modes

The initial parameter to be determined was related to the sizing of the power-screw motor. Sizing this motor involved calculating both the required motor force and torque. The size of the motor depended on the desired actuator force generated by the controller when it was in active mode. The specified range for the desired actuator force, F_a , falls between 73,620 and 159,180 N, as listed in Table 1. The DHIL actuator needed to be capable of generating a maximum force of 159,180 N to counteract load transfer. However, the actuator must be designed with a safety factor of 1.2 [37], [38] to account for potential vehicle overloading scenarios. Consequently, the DHIL actuator must be able to produce a maximum force of 191,016 N for motor sizing purposes. However, this maximum force would not affect the actuator force, as determined by the controller.

Table 1. The static and maximum desired actuator force during DHIL active mode

Semitrailer configuration			F_a static (N)	F_a max. (N)
20-foot	Half laden	BR20HL	73,620	87,316
container	Full laden	BR20FL	116,126	158,807
40-foot	Half laden	BR40HL	95,816	113,607
container	Full laden	BR40FL	118,302	159,180

The second parameter to be considered was the lifting height. A kinematic relationship existed between the vertical hitch displacement and the semitrailer’s pitch angle during harsh braking. The semitrailer bed tended to dive forward during braking, prompting the actuator to raise the semitrailer at the hitch point to level it back to its original position. Table 2 provides the results of the semitrailer’s pitch angle during a simulated 90 km/h braking test using a verified tractor-semi-trailer model and vehicle parameters published by Abdul Manaf et al. [9]. It is important to note that the pitch center is located at the semitrailer’s center of gravity, as depicted in Figure 5. The semitrailer would experience a pitch-

down angle ranging from 0.1270° to 0.4480°, which corresponded to a dive height between 12.75 and 45.46 mm. This dive height represented the amount by which the DHIL actuator needed to lift the hitch point back to its original static hitch height, denoted as the vertical displacement of the hitch coupling, H_3 . Consequently, the controller would command the actuator to elevate the hitch coupling based on the desired actuator force data, as discussed in the preceding paragraph.

Table 2. Semitrailer pitch angle of four types of configurations based on published data [9]

Semitrailer configuration (passive mode)			Pitch angle (°)			H_3 (mm)
			Minimum	Maximum	Range	
20-foot semitrailer	Half laden	BR20HL	-0.4185	0.0295	0.4480	35.97
	Full laden	BR20FL	-0.7125	-0.1463	0.5662	45.46
40-foot semitrailer	Half laden	BR20HL	-0.1534	-0.0573	0.0961	12.75
	Full laden	BR20FL	-0.2770	-0.1500	0.1270	16.85

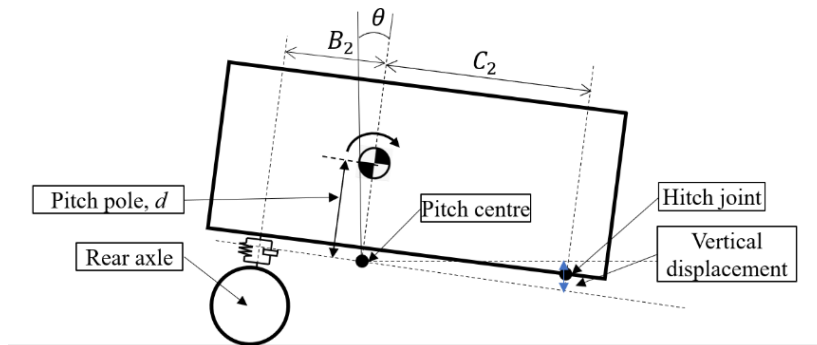


Figure 5. A semitrailer’s pitch-down occurs at the pitch center

Next, the appropriate motor size for the DHIL actuator’s operation was determined, whereby two crucial motor parameters that drive the DHIL actuator were motor torque and motor step count. Motor speeds were determined based on the motor torque, which signified the lifting power of the motor. On the other hand, motor step counts were derived from the hitch coupling displacement to ensure that the motor would stop at the desired height.

First, motor speeds were established by determining the relationship between hitch coupling displacement and the desired actuator force. The actuator force and hitch coupling displacement were two parameters connected through Hooke’s law. Each elevation of the hitch coupling by the actuator would produce the desired actuator force, as defined in Equation (5). Consequently, this relationship was assumed to have a linear correlation. Given the magnitude of the desired actuator force from the controller, the hitch coupling displacement can be determined. The equation parameters have been determined through regression analysis, as detailed in Table 3. Subsequently, the short arm angle, β'' , can be calculated, as defined in Equation (6). It is important to note that H'_3 represents the initial hitch coupling height when the DHIL actuator is in passive mode, as illustrated in Figure 6.

$$H_3 = \frac{F_a}{K} + \frac{C}{K} \tag{5}$$

$$\beta'' = \sin^{-1} \frac{H'_3 + H_3}{Q} \tag{6}$$

Table 3. Parameter values of Equation (5)

Semitrailer configuration			K	C
20-foot container	Full laden	BR20FL	883	85,200
	Half laden	BR20HL	176	116,000
40-foot container	Full laden	BR40FL	1,500	95,800
	Half laden	BR40HL	2,663	118,000

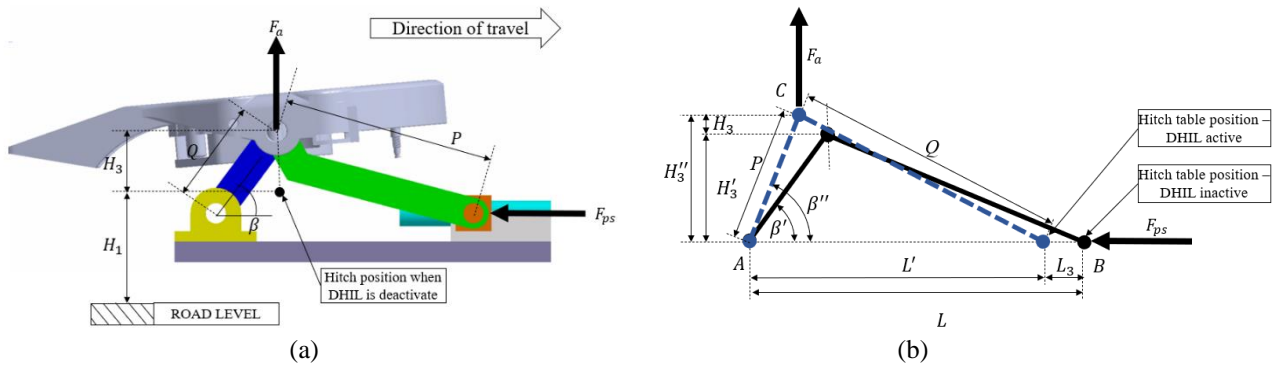


Figure 6. DHIL kinematics during operation: (a) lifting mechanism; and (b) free body diagram of DHIL kinematic points

Once the hitch coupling displacement has been determined, the motor torque and step counts can be calculated using a set of motor model equations. Initially, the actuator force was converted into the power screw force, denoted as F_{ps} , as defined in Equation (7). This relationship is established using the static moment method, relying on Figure 6 as a free-body diagram. By employing this equation, the maximum power screw force can be computed. In this context, the maximum actuator force of 191,016 N would lead to the maximum power screw force of 13,840 N.

$$F_{ps} = F_a \left[\frac{Q \cos \beta'' \tan \left\{ \arcsin \left(\frac{Q}{P} \sin \beta'' \right) \right\}}{P \cos \left\{ \arcsin \left(\frac{Q}{P} \sin \beta'' \right) \right\} + Q \cos \beta''} \right] \quad (7)$$

Subsequently, the power screw torque was established, as defined in Equation (8). This power screw torque was instrumental in elevating the hitch coupling to the desired height, as directed by the controller's command. It must be noted that the power screw was connected to the stepper motor, which meant that the power screw torque was equivalent to the motor torque. The power screw torque of the DHIL was based on the power-screw torque model introduced by Childs and Zhou *et al.* [39], [40]. In this model, the first term on the right-hand side represents the lead screw torque, while the second term accounts for the collar friction torque. The torque calculation primarily served to determine the maximum torque output required by the controller. Since the stepper motor's torque would remain constant, it would not play a role in actuating the controller. Instead, the model's purpose was to establish torque specifications. By applying this equation, the maximum torque generated by the motor can be computed. In this scenario, the maximum power screw force of 13,840 N would result in a maximum motor torque of 2000 Nm.

$$T_{ps} = \frac{F_{ps} d_s}{2} \left[\frac{l_s + \pi \mu_s d_s \sec \alpha}{\pi d_s - \mu_s l_s \sec \alpha} \right] + \frac{F_{ps} \mu_c d_c}{2} \quad (8)$$

After establishing the motor torque, the subsequent step involved determining the motor step counts. This process began by establishing the relationship between horizontal motor displacement, denoted as L_3 , and hitch coupling height, denoted as H_3 , as defined in Equation (9). This relationship is based on kinematic principles, as depicted in Figure 5. Following this, the motor step counts, as defined in Equation (10), relied on the screw pitch, denoted as l_s , and the motor steps per revolution, denoted as S_{psFull} . The ideal specifications for the DHIL actuator parameters are detailed in Table 4, encompassing three key components: actuator parameters, power screw parameters, and stepper motor parameters.

$$L_3 = 0.0043H_3^2 + 0.4149H_3 + 0.0036 \quad (9)$$

$$S_{psDes2} = \frac{1}{l_s} L_3 S_{psFull} \quad (10)$$

Table 4. Ideal specifications for the DHIL actuator

Motor and Power Screw Parameters	Value
Actuator Parameter	
Initial hitch coupling height, H_3'	55.00 mm
Max. actuator force, $F_{a,max}$	191,016 N
Max. lifting height, H_3'	42.50 mm
Power Screw Parameter	
Power Screw Type	ACME thread lead screw
Power-Screw Thread Angle, 2α	29°
Screw Means (Pitch) Diameter, d_s	35.00 mm

Table 4. (cont.)

Motor and Power Screw Parameters	Value
Collar Diameter, d_c	70.00 mm
Screw Friction, μ_s	0.15
Collar Friction, μ_c	0.15
Power-Screw Lead/Pitch, l_s	8.00 mm
Stepper Motor Parameter	
Input voltage, V_m	DC 48 V
Rated current, I_m	2 A
Rated Torque, T_{ps}	1545 Nm
Rated speeds, N_{ps}	1000 RPM (16.67 rev/s)
Stroke speeds	133.6 mm/s
Rated Power, P_m	96 W
Step angle / full step, S_{psFull}	1.8° / 200 steps

2.4 Optimization of controller gains using particle swarm optimization

The DHIL controller was incorporated with two adjustable controller parameters, denoted as K_{p1} and K_{p4} , along with three adjustable gains, specifically C_{Sky} , K_1 , and K_2 . These parameters underwent a tuning process through two optimization steps: the trial-and-error method and particle swarm optimization (PSO). Initially, the trial-and-error method was employed to determine the initial values of the five tuneable parameters. The initial values of these parameters were randomly assigned and changed until the controller had shown a sign of load transfer reduction. These values were established based on data derived from active vehicle simulations that were conducted during harsh braking scenarios. Subsequently, these values were further refined using the PSO method.

In the trial-and-error method, 10 different trial values are selected for each tuneable parameter to minimize the CRMS error in each run, as listed in Table 5. The CRMS error for the next run must be converged to obtain the optimum initial parameters and boundary parameters for the tuning process using PSO. The convergence of CRMS error is shown in Figure 7 where the local minima represent the initial parameter for PSO tuning. The initial parameters and boundary parameters are listed in Table 6.

Table 5. Results of the trial-and-error method for controller parameters

Parameter	#Run	Initial value	CRMS	Error (%)	Remarks
K_{p1}	1	1.42×10^6	3449	15.41%	Optimized value between 1.46×10^6 and 1.48×10^6
	2	1.43×10^6	3574	12.35%	
	3	1.44×10^6	3700	9.25%	
	4	1.45×10^6	3829	6.10%	
	5	1.46×10^6	3959	2.91%	
	6	1.47×10^6	4092	0.34%	
	7	1.48×10^6	4226	3.64%	
	8	1.49×10^6	4363	6.99%	
	9	1.50×10^6	4502	10.40%	
	10	1.51×10^6	3396	16.72%	
K_{p4}	1	1.3	1475	63.83%	Optimized value between 1.7 and 1.9
	2	1.4	2020	50.47%	
	3	1.5	2573	36.91%	
	4	1.6	3133	23.17%	
	5	1.7	3701	9.24%	
	6	1.8	4277	4.89%	
	7	1.9	4861	19.2%	
	8	2.0	5453	33.71%	
	9	2.1	6052	48.42%	
	10	2.2	6660	63.33%	

Table 5. Results of the trial-and-error method for controller parameters

Parameter	#Run	Initial value	CRMS	Error (%)	Remarks
C_{sky}	1	1×10^5	3235	20.68%	An optimized value between 5×10^5 and 7×10^5
	2	2×10^5	3395	16.75%	
	3	3×10^5	3558	12.74%	
	4	4×10^5	3725	8.66%	
	5	5×10^5	3895	4.49%	
	6	6×10^5	4068	0.24%	
	7	7×10^5	4245	4.11%	
	8	8×10^5	4426	8.54%	
	9	9×10^5	4611	13.07%	
	10	10×10^5	4799	17.69%	
K_1	1	6.9	3187	21.83%	Optimized value between 7.2 and 7.4
	2	7.0	4146	1.68%	
	3	7.1	4124	1.14%	
	4	7.2	4103	0.61%	
	5	7.3	4072	0.15%	
	6	7.4	4024	1.33%	
	7	7.5	3990	2.16%	
	8	7.6	3752	7.98%	
	9	7.7	2995	26.54%	
	10	7.8	2973	27.09%	
K_2	1	3.7	3593	11.89%	Optimized value between 4.1 and 4.3
	2	3.8	3690	9.52%	
	3	3.9	3792	7.01%	
	4	4.0	3900	4.36%	
	5	4.1	4014	1.56%	
	6	4.2	4136	1.42%	
	7	4.3	4265	4.58%	
	8	4.4	4402	7.94%	
	9	4.5	4548	11.53%	
	10	4.6	4705	15.37%	

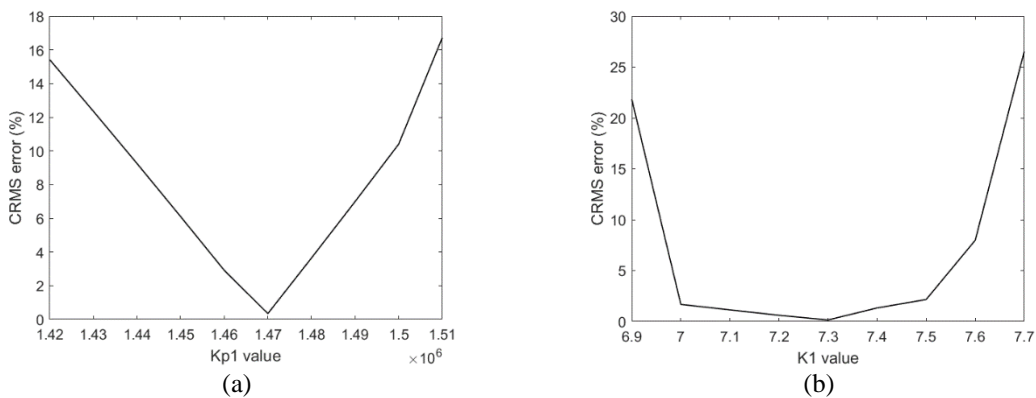


Figure 7. Local minima of tuneable parameters from 10 runs for (a) K_{p1} , (b) K_1

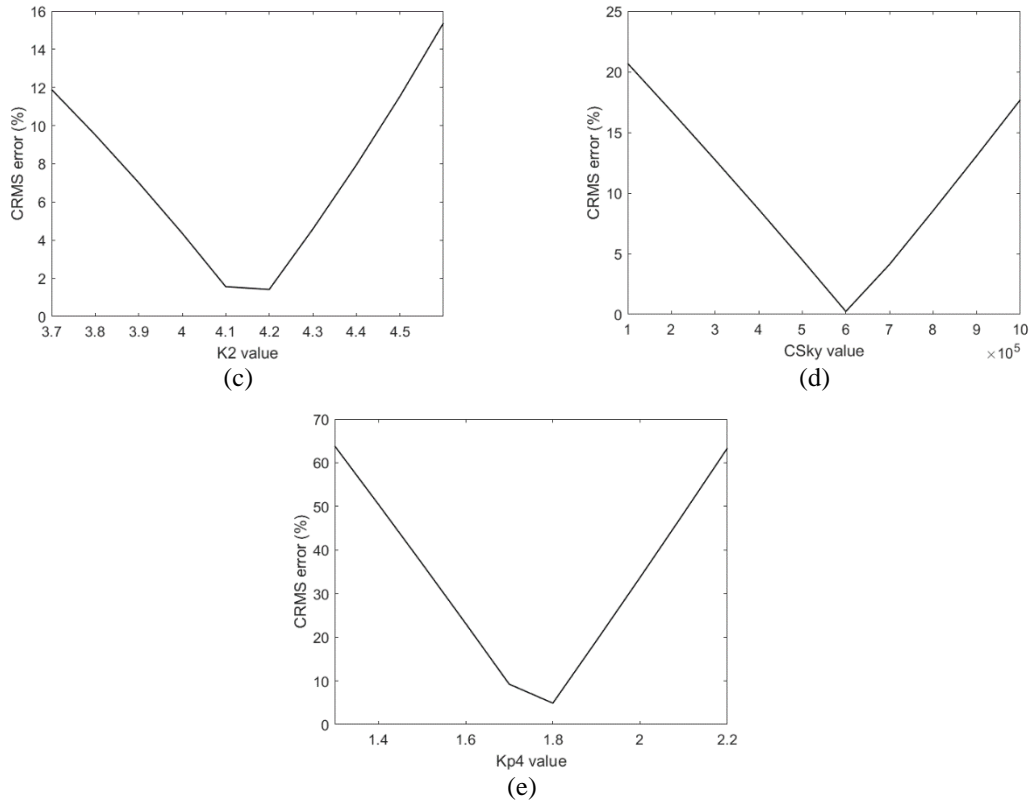


Figure 7. (cont.) (c) K_2 , (d) C_{sky} , and (e) K_{p4}

Table 6. Trial and error output to determine the initial data and boundary data of the PSO method

Coeff.	LB	Initial value	UB	Optimized value
K_{p1}	1.46×10^6	1.47×10^6	1.48×10^6	1474931.8330
K_1	7.2	7.3	7.4	7.3451
K_2	4.1	4.2	4.3	4.1227
C_{sky}	5×10^5	6×10^5	7×10^5	602089.9982
K_{p4}	1.7	1.8	1.9	1.7648

Once stable tuneable parameter values have been achieved, the fine-tuning process begins. The fine-tuning process involved using a metaheuristic controller optimization method, known as particle swarm optimization (PSO). PSO is a widely used approach for offline tuning procedures that aims to identify a set of parameters resulting in optimal controller performance. This study has also applied the PSO method, following a similar approach for parameter tuning, as presented in several studies [41] - [46].

The primary goal of the PSO optimization process was to minimize load transfer. Consequently, the PSO algorithm required a reference value to effectively execute the fitness function. In this context, the algorithm utilizes the 50% passive load transfer as a reference point, as outlined in Table 7. Load transfer is a critical component of the internal force system linked to the vehicle’s acceleration [9]. Reducing the load transfer by more than 50% would ultimately lead to a reduction in the force components, which, in turn, would lead to the vehicle’s deceleration. This increased deceleration, in turn, would result in an extended braking distance for the vehicle [47].

Table 7. Magnitude of semitrailer load transfer as PSO reference

Semitrailer configuration			Load transfer (N)	
			100%	50%
20-foot container	Half laden	BR20HL	36,100	18,050
	Full laden	BR20FL	48,400	24,200
40-foot container	Half laden	BR40HL	20,100	10,050
	Full laden	BR40FL	26,800	13,400

The PSO algorithm worked to optimize the gain parameter values starting from their initial settings, with the objective of achieving a load transfer response that would closely match the reference value. This optimization process involved minimizing a fitness function that would quantify the error in load transfer between the model and the reference value, as

described in Equation (11). In this scenario, the position of each particle would correspond to the variables being optimized, which in this case, amounted to five. The fitness of each particle was evaluated based on its controller performance value. The working process of PSO is shown in Figure 8.

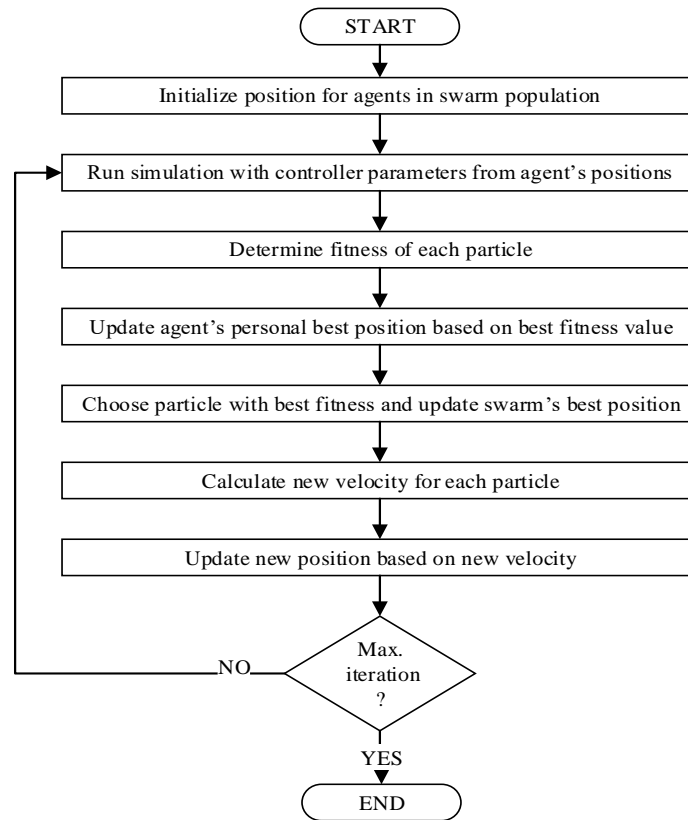


Figure 8. PSO procedure for DHIL controller [41]

The fitness function utilized by the PSO algorithm was constructed using the Cumulative Root Mean Square (CRMS) value, which compared the reference load transfer data, denoted as LT_{ref} , with the model load transfer data, denoted as LT_{model} . This algorithm would identify the particle with the best fitness, which was then compared with personal and global best records. Then, this algorithm would retain the position associated with the best-performing particle for use in subsequent iterations.

$$\begin{aligned}
 \text{Fitness function} &= f(K_{p1}, K_{p4}, K_1, K_2, C_{sky}) \\
 &= \sqrt{(CRMS(LT_{ref}))^2 - (CRMS(LT_{model}))^2} \tag{11}
 \end{aligned}$$

Furthermore, the optimization constraints encompassed the lower and upper limits of the tuneable parameters, thus, essentially defining the search space within which the PSO algorithm operated. This search space was confined within practical limits and these boundaries held significance in preventing the controller from entering an unstable mode, which could prematurely terminate the optimization process. Additionally, these limits have been instrumental in restricting the search space and facilitating a rapid convergence. Table 8 details the PSO parameters used in the optimization process. The optimization results for the five tuneable parameters are presented in Table 9.

Table 8. PSO parameters for controller optimization

PSO parameter	Value
Social coefficient, s	1.42
Cognitive coefficient, c	1.42
Inertial weight, iw	0.9
No. of variables (dimension), N_d	5
No. of particles, N_p	20
No. of iterations, N_i	20
Upper bound limit, UB	Refer to Table 6
Lower bound limit, LB	Refer to Table 6

Table 9. Final values of controller parameters obtained using the PSO method

Gain parameter	Value
K_{p1}	1474931.8330
K_1	7.3451
K_2	4.1502
C_{sky}	602089.9982
K_{p4}	1.7648

3.0 DHIL CONTROLLER STABILITY

In the development of this controller, the controller stability test was necessary to verify whether the operation zone of the controller was stable. The controller would evaluate the vehicle combinations consisting of multiple initial braking speeds, braking decelerations, load conditions, and semitrailer sizes. This approach was critical for identifying the controller’s limitations in various vehicle combinations. The following were three vehicle configurations to test the controller:

- a) The semitrailer load conditions followed a Maximum Permissible Laden Weight (MPLW) [48] between 10,000 (unladen) and 32,000 kg (full-laden) for a three-axle combination vehicle. Unladen was the weight of a tractor-semitrailer without cargo, while full-laden was the vehicle’s weight plus cargo.
- b) The initial vehicle speeds for braking were between 60 (low-speed braking) and 120 km/h (high-speed braking).
- c) The semitrailer size was either a 20-foot container semitrailer (7.6 m) or a 40-foot container semitrailer (13.6 m).

The load transfer responses were recorded using the CRMS value, as shown in Equation (12), where T is the entire simulation duration and $u(t)$ is the response signal data. It measured the RMS value continuously instead of at a discrete time.

$$CRMS = \sqrt{\frac{1}{T} \int_0^T \|u(t)\|^2 dt} \tag{12}$$

3.1 Different initial braking speeds

In the first stability test, a 40-foot container semitrailer was used and it maintained a consistent load condition of 32,000 kg. During this test, the initial braking speed was systematically varied starting from 60 km/h, with 20 km/h increments of up to 120 km/h. Table 10 and Figure 9 present the maximum CRMS values of load transfer, both in active and passive scenarios. Notably, the controller demonstrated stability for initial braking speeds ranging from 60 to 100 km/h. However, instability was observed in the controller when the initial braking speed reached 120 km/h. Across the entire speed range, the controller achieved an average load transfer reduction of 8.15%. Interestingly, the magnitude of load transfer reduction remained nearly consistent between each speed increment. These simulation results suggested that the load transfer reduction effect remained constant within the initial braking speed range of 60 to 100 km/h. Based on these findings, the controller’s operation was deemed stable at initial vehicle speeds ranging from 60 to 100 km/h. Thus, for the subsequent simulations, the initial braking speed was set at 90 km/h, which aligned with the speed specified by Salaani [49].

Table 10. The percentages of load transfer reductions are based on initial braking speeds

Semitrailer configuration			CRMS		Percentage reduction (%)
			Active mode	Passive mode	
40-foot container	Full-laden	60–0 km/h	24,680	26,860	8.12%
	Full-laden	80–0 km/h	24,660	26,850	8.16%
	Full-laden	100–0 km/h	24,640	26,830	8.16%
	Full-laden	120–0 km/h	Unstable	26,800	Unstable

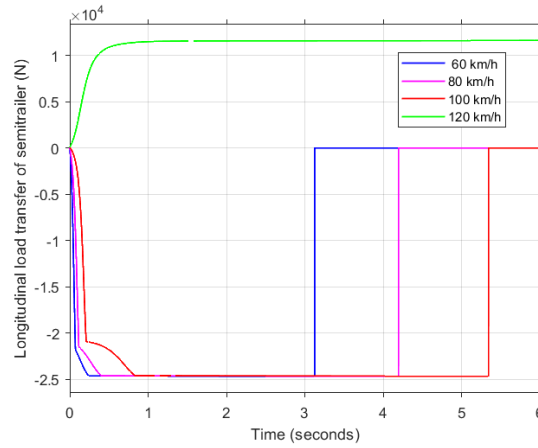


Figure 9. Controller stability test with different initial braking speeds in active mode

3.2 Different Braking Deceleration

The second stability test also used a 40-foot container semitrailer, with the initial braking speed consistently set at 90 km/h. Throughout this test, three different braking decelerations were examined, which were 0.6g braking (5.89 m/s²), 0.65g braking (6.38 m/s²), and 0.72g braking (7.06 m/s²). The results, as presented in Table 11, depict the percentage of load transfer reductions that have been achieved by the active mode of the vehicle. Figure 10 provides an overview of the controller’s stability test under different braking decelerations in the active mode. The results showed that the controller was stable during braking deceleration of greater than 0.5g. Notice that for emergency braking, the braking deceleration must be greater than 0.5g. Hence, the braking deceleration of less than 0.5g was not tested, as it would not achieve the objective of this study, which was to reduce the load transfer during emergency braking.

Table 11. The percentages of load transfer reductions are based on different braking decelerations

Semitrailer configuration			Deceleration (g)	CRMS		Percentage reduction (%)
				Active mode	Passive mode	
20-foot container	Full-laden	90–0 km/h	0.60	16,313	18,100	9.87%
	Full-laden	90–0 km/h	0.65	32,800	36,100	9.14%
	Full-laden	90–0 km/h	0.72	44,300	48,400	8.47%
40-foot container	Full-laden	90–0 km/h	0.60	9,208	10,120	9.01%
	Full-laden	90–0 km/h	0.65	18,400	20,100	8.46%
	Full-laden	90–0 km/h	0.72	24,700	26,800	7.84%

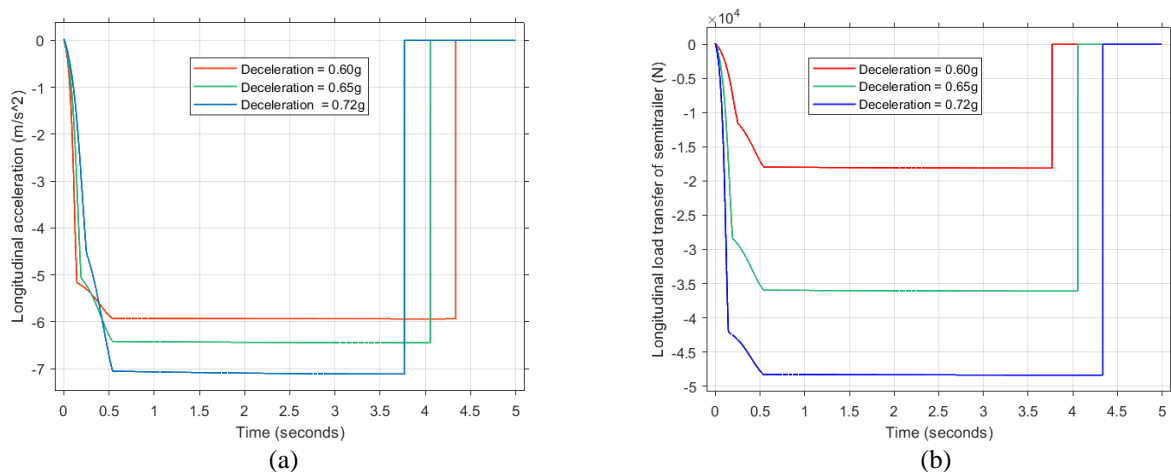


Figure 10. Controller stability test on different braking decelerations in active mode: (a) different braking decelerations for a 20-foot semitrailer; (b) longitudinal load transfer of semitrailer responses for a 20-foot semitrailer

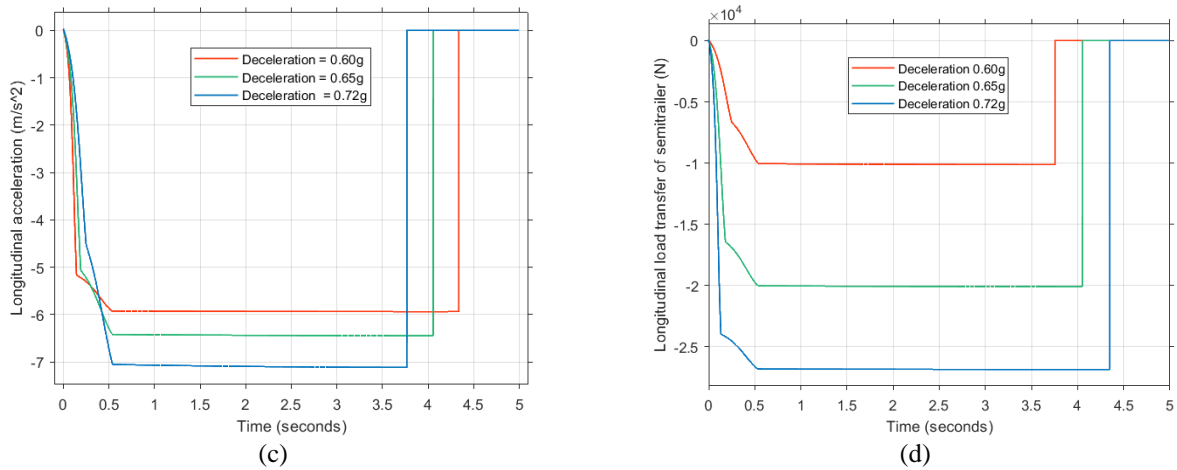


Figure 10. (cont.) (c) different braking decelerations for a 40-foot semitrailer and (d) longitudinal load transfer of semitrailer responses for a 40-foot semitrailer

3.3 Different load conditions

In the third stability test, a 40-foot container semitrailer was used, while the initial braking speed was consistently set at 90 km/h. Throughout this test, three different semitrailer load conditions were examined, which were 10,000 kg (unladen), 22,000 kg (half-laden), and 32,000 kg (full-laden). The results, as presented in Table 12, depict the percentages of load transfer reductions achieved by the active mode of the vehicle. Figure 11 provides an overview of the controller’s stability test under different load conditions in the active mode. For both the 20-foot and 40-foot semitrailers, the controller has demonstrated stability, exclusively when each semitrailer was half-laden or fully laden. However, instability was observed when the semitrailer was unladen. In this case, the vehicle failed to reach the stopping velocity and the positive load transfer indicated that the vehicle was in an acceleration mode rather than in a deceleration mode. Furthermore, the impact of load transfer in the unladen semitrailer was insignificant due to the absence of cargo. It would be worth noting that the load transfer in the unladen configuration was only 37% of the load transfer observed in the fully laden scenario. Therefore, the controller’s instability in the unladen semitrailer condition can be deemed acceptable.

Table 12. The percentages of load transfer reductions are based on different semitrailer load conditions

Semitrailer configuration			CRMS		Percentage reduction (%)
			Active mode	Passive mode	
20-foot container	Unladen	90–0 km/h	Unstable	18,100	Unstable
	Half laden	90–0 km/h	32,800	36,100	9.14%
	Full laden	90–0 km/h	44,300	48,400	8.47%
40-foot container	Unladen	90–0 km/h	Unstable	10,120	Unstable
	Half laden	90–0 km/h	18,400	20,100	8.46%
	Full laden	90–0 km/h	24,700	26,800	7.84%

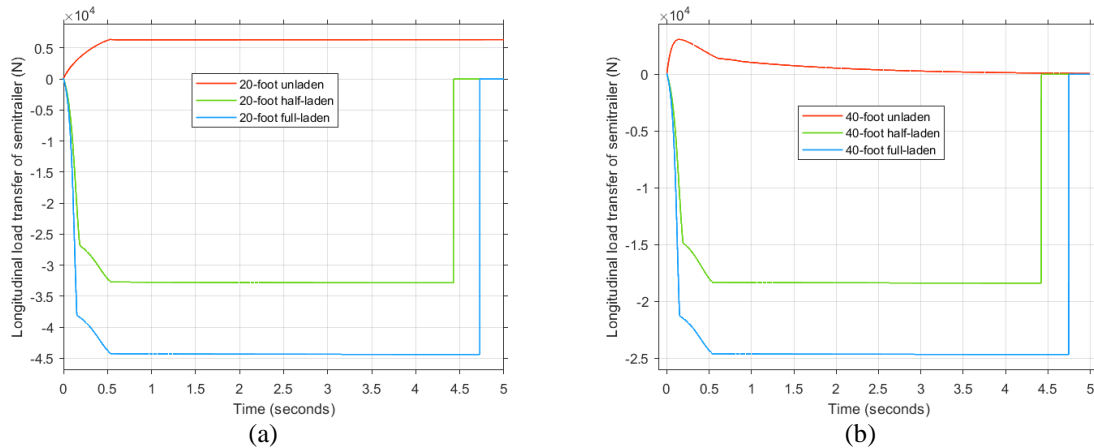


Figure 11. Controller stability test on different load conditions in active mode: (a) longitudinal load transfer of semitrailer responses for a 20-foot semitrailer; and (b) longitudinal load transfer of semitrailer responses for a 40-foot semitrailer

3.4 Different semitrailer sizes

In the fourth stability test, the load conditions remained constant at fully laden (32,000 kg), while the initial braking speed was consistently set at 90 km/h. This model was varied concerning two semitrailer size parameters: 20-foot and 40-foot semitrailer wheelbases. The maximum load transfer values, both in active and passive modes, are recorded in Table 13 and visualized in Figure 12. The controller was able to achieve an average load transfer reduction of 8.16% and effectively reduced load transfer in two different semitrailer sizes. It would be worth noting that the shorter semitrailer exhibited a greater reduction in load transfer compared to the longer wheelbase semitrailer. This disparity can be attributed to the wheelbase acting as a moment arm and generating a higher counterforce to mitigate load transfer. Although the load transfer reduction patterns were similar for both semitrailer sizes, the magnitudes of the load transfer reductions were varied. These findings indicated that different semitrailer sizes influence the load transfer reduction. In the case of the longer semitrailer, the controller’s capability to reduce load transfer was somewhat diminished due to the increased pitch moment resulting from the longer wheelbase length. However, overall, the controller remained stable in both semitrailer sizes.

Table 13. The percentages of load transfer reductions are based on different semitrailer sizes

Semitrailer configuration			CRMS		Percentage reduction (%)
			Active mode	Passive mode	
20-foot container	Full laden	90–0 km/h	44,300	48,400	8.47%
40-foot container	Full laden	90–0 km/h	24,700	26,800	7.84%

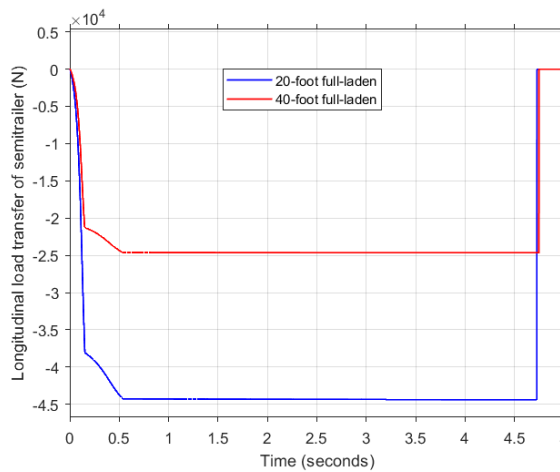


Figure 12. Controller stability test on different semitrailer sizes in active mode

The controller’s stability has been examined across three different vehicle configurations, encompassing variations in initial braking speeds, braking deceleration, load conditions, and semitrailer sizes. The test outcomes indicated that the controller was able to maintain stability in specific vehicle configurations while achieving load transfer reductions that ranged from 7.84% to 9.14%. A concise summary of the stable parameters for the DHIL controller is provided in Table 14.

Table 14. A summary of the stable region of the DHIL controller

Parameters	Minimum	Maximum
Initial braking speeds	60 km/h	100 km/h
Braking deceleration	0.5g	0.72g
Load condition	Half laden (22,000 kg)	Full laden (32,000 kg)
Semitrailer size	20-foot semitrailer	40-foot semitrailer

4.0 DHIL CONTROLLER PERFORMANCE BASED ON THE BRAKING TEST

The discussion in this section will revolve around the performance of the Dynamic Hitch Lift (DHIL) system by considering both vehicle dynamics and actuator response during braking tests. The primary data during braking maneuvers have been derived from the driver’s braking signal, while the DHIL system utilized the deceleration data to

distinguish between standard and harsh braking events. Specifically, braking with deceleration greater than 0.5g was classified as harsh braking, which would be equivalent to 150 MPa of brake pressure [50] - [54]. It is essential to emphasize that the energy required for braking remained constant across all speed settings. Throughout these test scenarios, the assumption was that the vehicle would accelerate solely in the longitudinal direction, without any steering input. Consequently, this study did not consider vehicle responses in the lateral direction. It should be clarified that the aim of the load transfer reduction system was not to bring the vehicle to a complete stop. Instead, the traditional mechanical brake system remained responsible for the final and permanent stopping of the tractor-semitrailer. The primary function of the DHIL system was to rapidly mitigate load transfer in the critical initial milliseconds following the driver’s application of the brakes.

This section has been divided into two primary performance categories: vehicle dynamic responses and actuator dynamic responses. The examination of vehicle dynamics involved a comparison between passive and active vehicles by considering different aspects, such as longitudinal load transfer, semitrailer pitch angle, semitrailer pitch rate, and vertical hitch force responses. The performance index for the vehicle dynamic responses was used to evaluate the active system’s ability to reduce load transfer in comparison to the passive system. In contrast, the actuator dynamic responses pertained to the performance analysis of the DHIL actuator, including aspects of actuator force responses, power-screw responses, and motor responses. The simulation results will be presented and assessed in the subsequent sections by employing visual comparison techniques [1], [55] - [57] and CRMS error analysis [15], [42], [58] - [60]. The performance of the controller has been observed across three distinct vehicle configurations, categorized as follows and as listed in Table 15:

- a) Semitrailer sizes were either 20-foot long (7.6 m wheelbase) or 40-foot long (13.6 m wheelbase).
- b) Semitrailer load conditions were either half-laden (22,000 kg) or full-laden (32,000 kg).
- c) The initial braking speed was constant at 90 km/h based on similar controller responses for 60 and 120 km/h breaking speeds.

Table 15. Tractor-semitrailer different configuration settings

Configuration name	Semitrailer size	Semitrailer load condition	Initial braking speed (km/h)
BR20FL	20-foot	Full laden	90–0
BR20HL	20-foot	Half laden	90–0
BR40FL	40-foot	Full laden	90–0
BR40HL	40-foot	Half laden	90–0

4.1 Performances of active and passive tractor-semitrailers based on the braking test

This section will discuss four categories of dynamic vehicle responses, encompassing longitudinal velocity, braking distance, semitrailer longitudinal load transfer, semitrailer pitch angle, semitrailer pitch rate, and vertical hitch forces. To facilitate a better understanding of vehicle responses in terms of load transfer, pitch angle, and pitch rate, the primary focus of this study is on the longitudinal velocity response, as illustrated in Figure 13. The impact of load transfer on braking distance and stopping time was also analyzed, which were vital aspects of vehicle performance. Data concerning the extension of braking distance and the delay in stopping time are detailed in Table 16. Notably, these vehicles experience delays in stopping time while in the active mode, averaging 0.38 s compared to the passive mode, as listed in Table 17. Furthermore, there was an extension in the braking distance of the active mode vehicles, averaging an increase of 4.85 m compared to the passive mode vehicles. These outcomes were logical, as the reduction in load transfer could also lead to a reduction in longitudinal acceleration.

Table 16. Longitudinal braking distance of different semitrailer configurations

Semitrailer configuration			Braking distance (m)		Distance extension (m)
			Active mode	Passive mode	
20-foot container	Half laden	BR20HL	56.80	52.40	4.40
	Full laden	BR20FL	61.90	56.90	5.00
40-foot container	Half laden	BR40HL	57.40	52.70	4.70
	Full laden	BR40FL	61.10	55.80	5.30

Table 17. Stopping time of different semitrailer configurations

Semitrailer configuration			Stopping time (s)		Stopping time delay (s)
			Active mode	Passive mode	
20-foot container	Half laden	BR20HL	4.39	4.06	0.33
	Full laden	BR20FL	4.73	4.33	0.4
40-foot container	Half laden	BR40HL	4.42	4.06	0.36
	Full laden	BR40FL	4.77	4.36	0.41

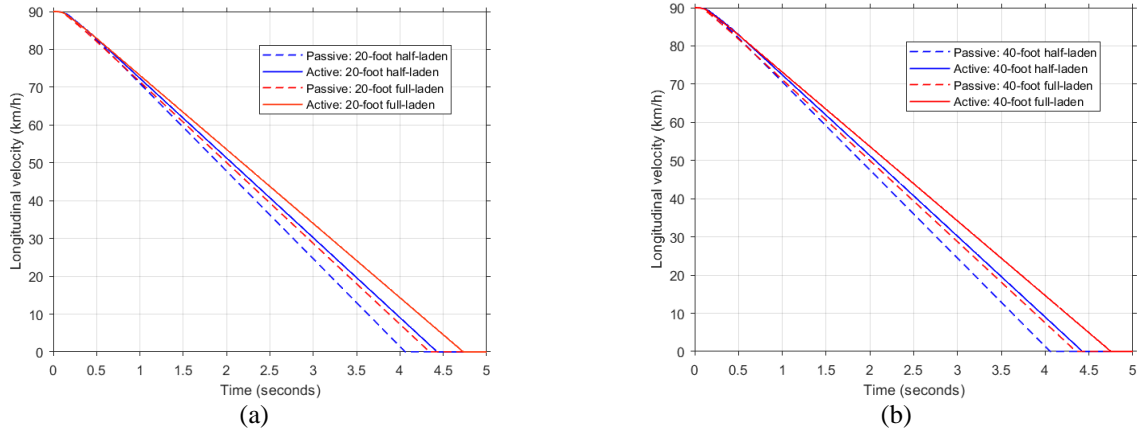


Figure 13. The longitudinal velocity of different semitrailer configurations in active and passive modes: (a) 20-foot semitrailer’s longitudinal velocity and (b) 40-foot semitrailer’s longitudinal velocity

The DHIL controller has also effectively reduced the longitudinal load transfer responses across all vehicle configurations, as outlined in Table 18. The longitudinal load transfer responses for different loads and semitrailer sizes are visually depicted in Figure 14. These findings demonstrated that the DHIL system can reduce load transfer, with an average reduction of 8.48%, as observed across all vehicle configurations. The load transfer patterns for active and passive vehicles exhibited similarities, even with differing load transfer magnitudes. Additionally, the 20-foot semitrailer exhibited a higher load transfer reduction capability compared to the 40-foot semitrailer. This disparity can be attributed to the shorter wheelbase of the 20-foot semitrailer, necessitating a higher actuator force to achieve a similar pitch moment.

Table 18. Longitudinal load transfer reduction percentages in different semitrailer configurations

Semitrailer configuration			CRMS		Reduction value (%)
			Active mode	Passive mode	
20-foot container	Half laden	BR20HL	32,800	36,100	9.14%
	Full laden	BR20FL	44,300	48,400	8.47%
40-foot container	Half laden	BR40HL	18,400	20,100	8.46%
	Full laden	BR40FL	24,700	26,800	7.84%

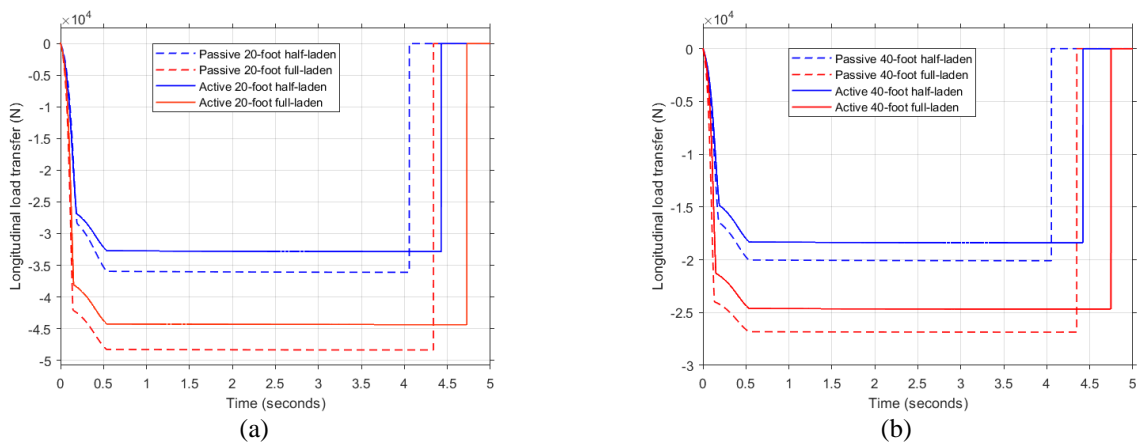


Figure 14. Longitudinal load transfer of different semitrailer configurations in active and passive modes: (a) 20-foot semitrailer’s load transfer and (b) 40-foot semitrailer’s load transfer

The DHIL controller has also effectively mitigated pitch angle variations across all vehicle configurations. The semitrailer pitch angle responses for different loads and semitrailer sizes are summarised in Table 19 and visually represented in Figure 15. The pitch angle reduction was within the range of 3.75% to 9.15% for all vehicle configurations. Interestingly, half-laden vehicles exhibited an average pitch angle reduction of 7.24%, which was higher compared to full-laden vehicles, with an average reduction of 5.86%. A positive pitch indicated that the vehicle was pitching downward, while a negative pitch signified an upward pitch. The proposed control strategy within the DHIL system has effectively stabilized these vehicles by reducing pitch angles and mitigating load transfer. However, the 40-foot semitrailer has exhibited more noticeable pitch angles due to its heavier load.

Table 19. Reduction percentages of semitrailer pitch angles in different semitrailer configurations

Semitrailer configuration			CRMS		Reduction value (%)
			Active mode	Passive mode	
20-foot container	Half laden	BR20HL	0.0299	0.0329	9.12%
	Full laden	BR20FL	0.0809	0.0879	7.96%
40-foot container	Half laden	BR40HL	0.1692	0.1788	5.36%
	Full laden	BR40FL	0.2646	0.2749	3.75%

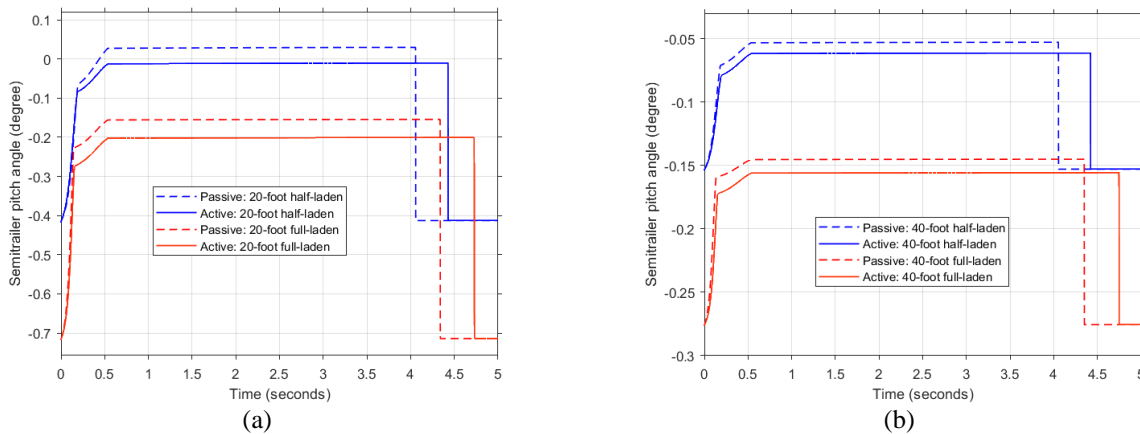


Figure 15. Semitrailer pitch angle at different configurations in active and passive modes: (a) 20-foot semitrailer’s pitch angle and (b) 40-foot semitrailer’s pitch angle

The DHIL controller is also able to mitigate pitch rate variations across all vehicle configurations, as depicted in Table 20. The results on semitrailer pitch rates for different loads and semitrailer sizes are illustrated in Figure 16 for the 20-foot semitrailer and in Figure 17 for the 40-foot semitrailer. In the active system, the pitch rate reduction ranged from 1.98% to 20.06% across all vehicle configurations. Although the active system has successfully reduced the pitch rate, there was a slight delay of approximately 0.02 s in reaching the steady state. This delay was considered negligible due to its small value. It must be emphasized that the semitrailer pitch rate served as a disturbance parameter that the DHIL controller has effectively rejected. This result has highlighted the controller’s ability to efficiently stabilize the vehicle during harsh braking scenarios.

Table 20. Reduction percentages of semitrailer pitch rates in different semitrailer configurations

Semitrailer configuration			CRMS		Reduction value (%)
			Active mode	Passive mode	
20-foot container	Half laden	BR20HL	0.1526	0.1909	20.06%
	Full laden	BR20FL	0.2768	0.3133	11.65%
40-foot container	Half laden	BR40HL	0.0812	0.0851	4.58%
	Full laden	BR40FL	0.1679	0.1713	1.98%

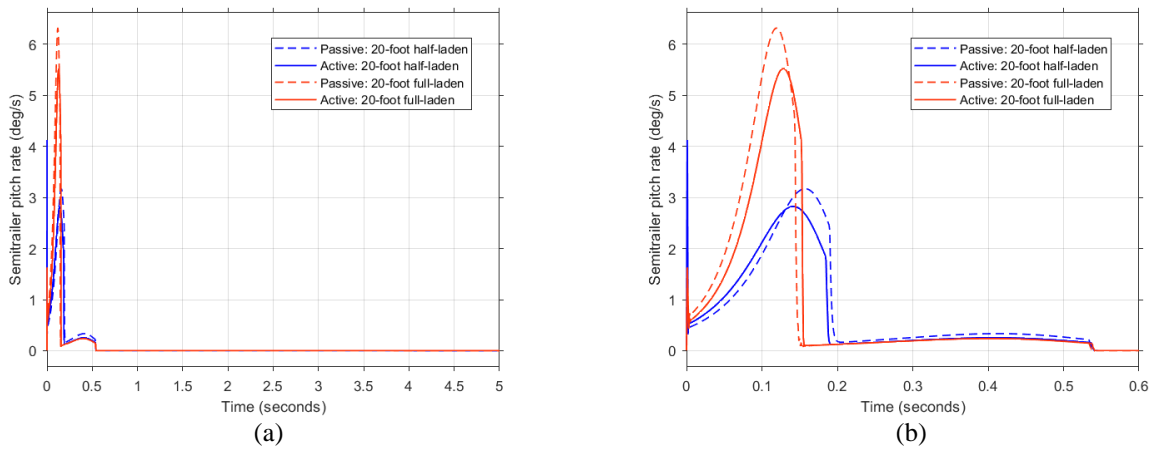


Figure 16. Semitrailer pitch rate of an active and passive system for a 20-foot semitrailer: (a) full data range of semitrailer pitch rates and (b) zoom-in displacement rate between 0 and 0.6 s

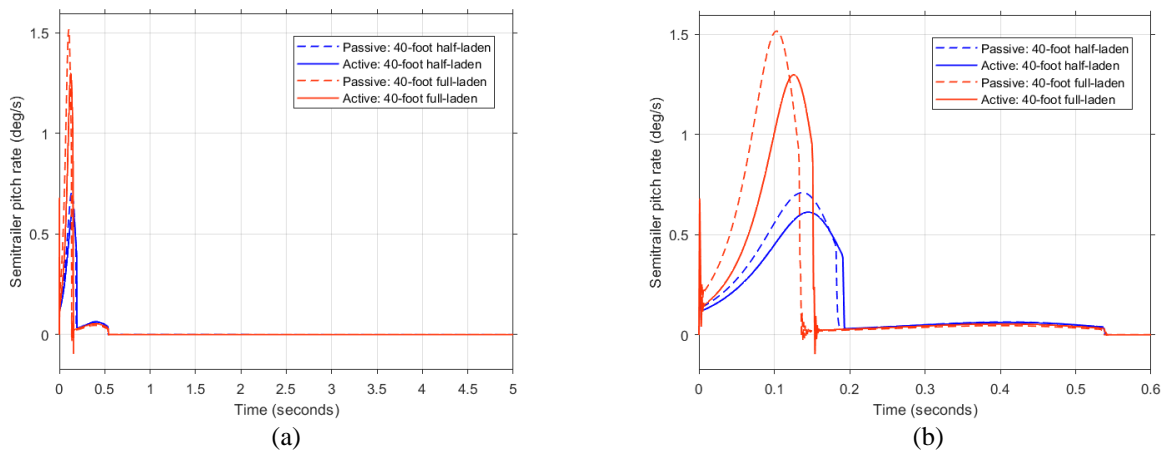


Figure 17. Semitrailer pitch rate of an active and passive system for a 40-foot semitrailer: (a) full data range of semitrailer pitch rates and (b) zoom-in displacement rates between 0 and 0.6 s

In terms of the vertical hitch force, it is evident that the DHIL controller has effectively reduced this force across all vehicle configurations, as summarised in Table 21. The results of vertical hitch force for different loads and semitrailer sizes are visually depicted in Figure 18. The reduction in vertical hitch force ranged from 1.12% to 2.25% across all vehicle configurations. The vertical hitch force response rapidly approached a steady state phase in all vehicle configurations. The vertical hitch force represented the resultant force acting on the hitch joint. In a passive system, this force comprised the static vertical force and longitudinal load transfer elements only. In contrast, within an active system, the DHIL controller would introduce the actuator force component into the vertical hitch force to counterbalance the load transfer by reducing pitch rate and pitch moment. This load transfer reduction mechanism, involving the actuator force, would render the force magnitudes between the passive and active systems nearly identical.

Table 21. Vertical hitch force reduction percentages in different semitrailer configurations

Semitrailer configuration			CRMS		Reduction value (%)
			Active mode	Passive mode	
20-foot container	Half laden	BR20HL	121,400	124,200	2.25%
	Full laden	BR20FL	165,200	168,700	2.07%
40-foot container	Half laden	BR40HL	118,000	119,500	1.26%
	Full laden	BR40FL	167,000	168,900	1.12%

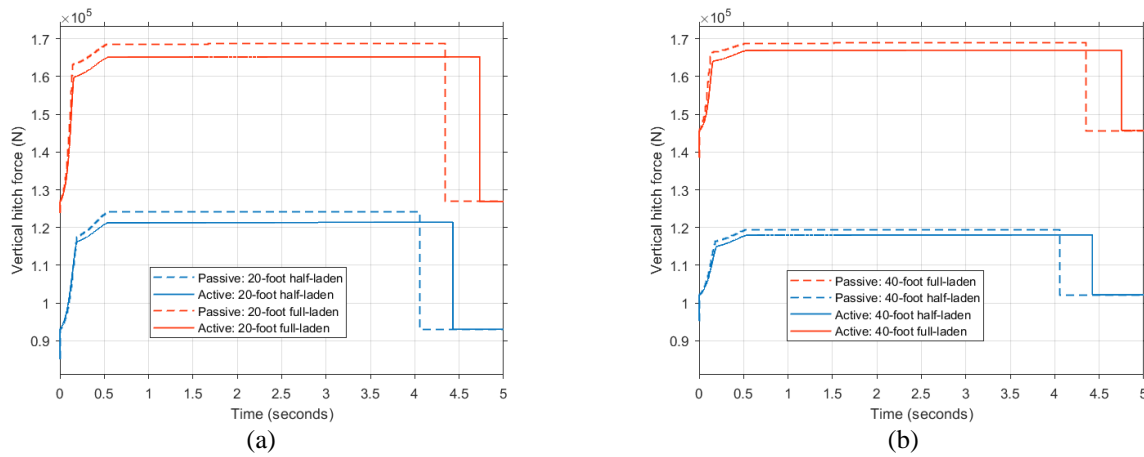


Figure 18. Vertical hitch force of different semitrailer configurations active and passive modes: (a) 20-foot semitrailer and (b) 40-foot semitrailer

4.2 DHIL actuator performance

This section will discuss the DHIL actuator performance, which consists of the vertical displacement and displacement rate of the hitch coupling, the desired actuator force, motor torque, motor step counts, and motor revolution angle. In terms of the vertical displacement of the hitch coupling, the DHIL controller has actively operated the hitch mechanism to elevate the hitch coupling during active mode. The displacement profile is visually represented in Figure 19, while the maximum displacement values are itemized in Table 22. Notably, the 20-foot semitrailer was able to raise the hitch coupling by an average of 40.72 mm, whereas the 40-foot semitrailer achieved a less substantial elevation, averaging merely 14.80 mm. This discrepancy in displacement can be attributed to the wider pitch angle range between static and maximum pitch angles exhibited by the 20-foot semitrailer compared to the 40-foot variant.

Table 22. Maximum vertical displacement of hitch coupling in different load conditions and semitrailer sizes based on the braking tests

Semitrailer configuration			Displacement (mm)
20-foot semitrailer	Half laden	BR20HL	35.97
	Full laden	BR20FL	45.46
40-foot semitrailer	Half laden	BR40HL	12.75
	Full laden	BR40FL	16.85

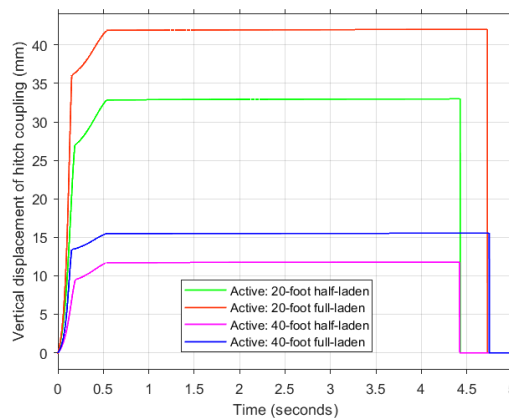


Figure 19. Vertical displacement of hitch coupling in different load conditions and semitrailer sizes based on the braking tests

In terms of the hitch coupling displacement rate, the DHIL controller was able to activate the hitch mechanism to raise the hitch coupling in the active mode. The displacement rate profile is depicted in Figure 20, while the maximum displacement rates at specific time points are detailed in Table 23. Notably, the 20-foot semitrailer, with its greater displacement, required a more rapid rate of elevation by the actuator to achieve a similar settling time as the 40-foot semitrailer. These data can be utilized to determine the maximum stroke speed of the power screw.

Table 23. Maximum vertical displacement rates of hitch coupling in different load conditions and semitrailer sizes based on the braking tests

Semitrailer configuration			Displacement rate (mm/s)
20-foot semitrailer	Half laden	BR20HL	231.43 at 0.14 s
	Full laden	BR20FL	451.42 at 0.13 s
40-foot semitrailer	Half laden	BR40HL	77.37 at 0.15 s
	Full laden	BR40FL	168.06 at 0.13 s

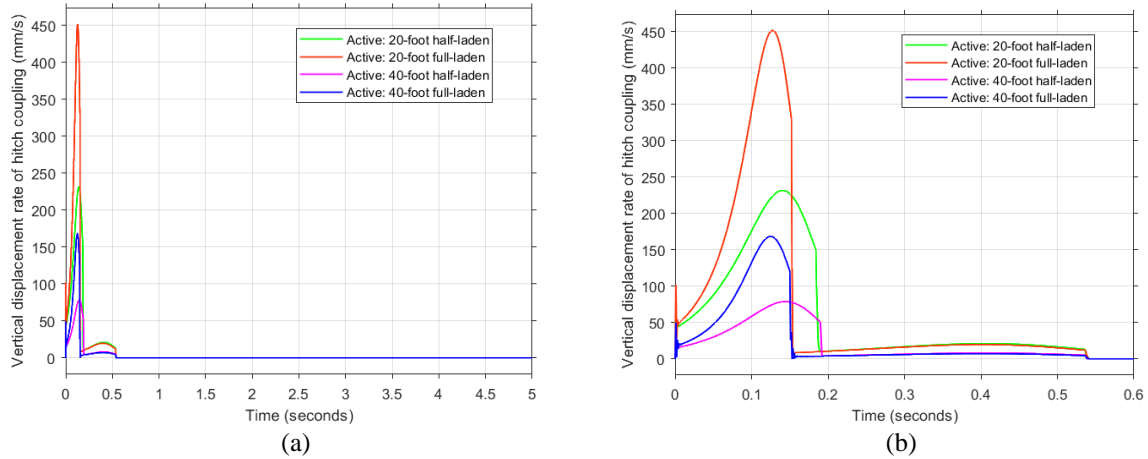


Figure 20. Vertical displacement rates of hitch coupling in different load conditions and semitrailer sizes based on the braking tests: (a) full data range of the displacement rates and (b) zoom-in displacement rates between 0 and 0.6 s

Meanwhile, the actuator force represented the force generated by the DHIL controller to counteract the load transfer. It is important to note that the magnitude of the actuator force was consistently lower than that of the vertical hitch force since the actuator force was integrated into the vehicle’s internal force system. Table 24 and Figure 21 present the actuator force responses for four different semitrailer combinations. The maximum magnitude of actuator force was 159,197 N for a full-laden 40-foot combination vehicle, while the lowest magnitude was 87,322 N for a half-laden 20-foot vehicle. These data would be utilized to determine the performance characteristics of the power screw, which were discussed with the DHIL actuator model in the preceding section.

Table 24. Maximum actuator force in different load conditions and semitrailer sizes based on the braking tests

Semitrailer configuration			Actuator force (N)
20-foot semitrailer	Half laden	BR20HL	87,322
	Full laden	BR20FL	158,801
40-foot semitrailer	Half laden	BR40HL	113,603
	Full laden	BR40FL	159,197

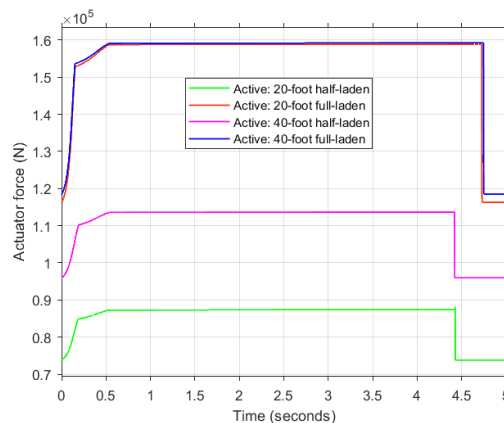


Figure 21. Actuator force responses for different load conditions and semitrailer sizes based on the braking tests

Table 25 shows the maximum magnitude of electric motor torque required to operate the DHIL system. Across all scenarios, the highest demanded motor torque was 1,695 Nm, while the lowest was 857 Nm. The increasing load conditions have led to higher vertical forces, resulting in an elevated demand for motor torque, as illustrated in Figure 22. Additionally, the longer semitrailers with identical load conditions would generate greater moments, thus, necessitating higher torques from the motor to engage the DHIL system. This study has employed the maximum simulated motor torque values to design a motor-gear train system for the DHIL actuator. The substantial torque values necessitated a larger motor, but this may be impractical for installation on the tractor chassis. Therefore, a smaller electric motor must be paired with a high-torque transmission system to achieve a comparable torque magnitude. According to the simulation, a maximum motor speed of 1,000 rpm will produce an equivalent torque of 1,695 Nm.

Table 25. The required maximum motor torque to actuate the DHIL system

Semitrailer configuration			Motor torque (N)
20-foot semitrailer	Half laden	BR20HL	857
	Full laden	BR20FL	857
40-foot semitrailer	Half laden	BR40HL	1266
	Full laden	BR40FL	1695

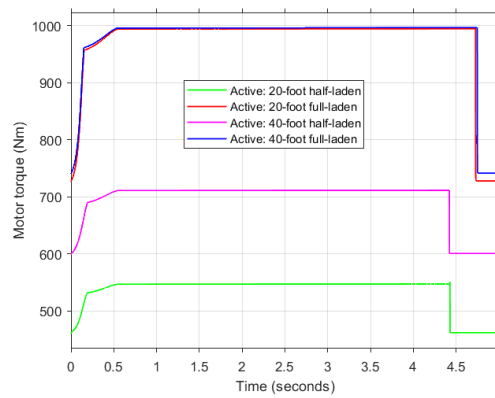


Figure 22. The generated electric motor torques from different load conditions and semitrailer sizes

In terms of the number of motor step counts, the DHIL actuator would issue commands to the motor to rotate a specific number of steps. The command profile is depicted in Figure 23, and the maximum step counts are detailed in Table 26. This command profile was subsequently translated into a digital pulse width modulation (PWM) signal for the motor to execute. The PWM signal will be presented in the next study involving hardware-in-the-loop. The patterns in the step count mirrored the responses of the actuator parameters.

Table 26. Maximum number of motor steps in different load conditions and semitrailer sizes based on the braking tests

Semitrailer configuration			Number of steps
20-foot semitrailer	Half laden	BR20HL	456
	Full laden	BR20FL	627
40-foot semitrailer	Half laden	BR40HL	137
	Full laden	BR40FL	187

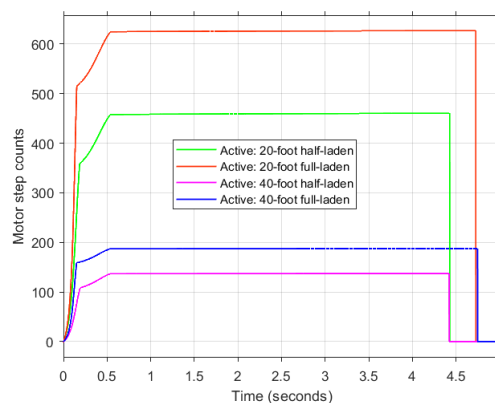


Figure 23. Number of motor steps for different load conditions and semitrailer sizes based on the braking tests

The motor revolution angle has a similar dataset to motor step counts but has been expressed as revolution angles. To derive this command, the motor step counts were multiplied by a step angle of 1.8°. Figure 24 illustrates the motor revolution angle profile, and the maximum angle values are listed in Table 27.

Table 27. Maximum rotation angles in different load conditions and semitrailer sizes based on the braking tests

Semitrailer configuration			Angle (°)
20-foot semitrailer	Half laden	BR20HL	823
	Full laden	BR20FL	1127
40-foot semitrailer	Half laden	BR40HL	247
	Full laden	BR40FL	337

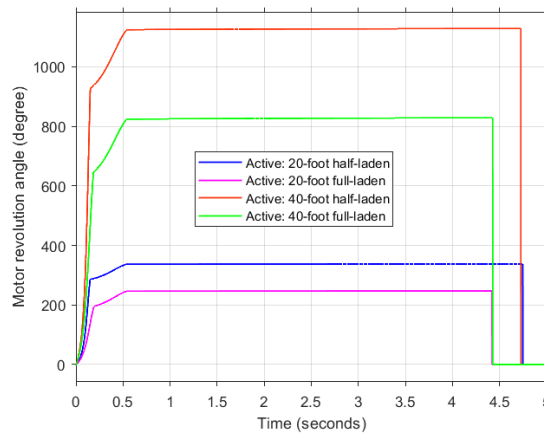


Figure 24. Motor revolution angles for different load conditions and semitrailer sizes based on the braking tests

5.0 CONCLUSIONS

This study aimed to develop a new hybrid control strategy for the Dynamic Hitch Lift (DHIL) actuator system that could reduce the longitudinal load transfer in a tractor-semitrailer. Subsequently, the load transfer was efficiently reduced by the control strategy using pitch rate reduction and pitch moment rejection, with Skyhook moment assist. The controller parameters were selected using the trial-and-error method based on the sensitivity analysis and were optimized using the PSO method. A tractor-semitrailer model with 12 degrees of freedom was used in the study to test the PSO-tuned controller based on harsh braking tests in different vehicle configurations.

The dynamic vehicle responses between the active and passive systems showed that the hybrid control strategy proposed in this study has efficiently reduced the longitudinal load transfer. The DHIL control strategy was able to reduce the load transfer up to 9.14%. The load transfer reduction has also affected the semitrailer pitch angle and pitch rate, as well as the vertical hitch force by 9.12%, 20.06%, and 2.25%, respectively. The reduction of semitrailer pitch angle and pitch rate was able to stabilize the vehicle, while the reduction in vertical hitch force normalized the longitudinal load transfer.

The actuator dynamic responses have shown that the maximum reduction of 9.14% of load transfer required the power screw of the DHIL actuator to generate a maximum of 1,695 Nm of torque at a constant motor speed of 1,000 rpm. This condition led the lifting mechanism of the DHIL actuator to produce a maximum of 159,157 N of counterforce to reduce the load transfer. In conclusion, the proposed DHIL controller has been optimized and stable in reducing the longitudinal load transfer in heavy combination vehicles during harsh braking. For future work, it was evident that the controller performance in different initial braking speeds would be insignificant due to the PID type controller in this study. However, the use of a speed-sensitive controller, for example, an Adaptive-PID could significantly affect the initial braking speed and the controller’s capability to reduce load transfer.

6.0 ACKNOWLEDGEMENT

The authors would like to express their gratitude to the Universiti Teknikal Malaysia Melaka (UTeM) and the Ministry of Higher Education Malaysia for supporting and funding this study.

7.0 REFERENCES

- [1] F. Ahmad, K. Hudha, F. Imaduddin, and H. Jamaluddin, “Modelling, validation and adaptive PID control with pitch moment rejection of active suspension system for reducing unwanted vehicle motion in longitudinal direction,” *International Journal of Vehicle Systems Modelling and Testing*, vol. 5, no. 4, pp. 312–346, 2010.

- [2] F. Bin Ahmad, K. Hudha, and H. Jamaluddin, "Gain scheduling PID control with pitch moment rejection for reducing vehicle dive and squat," *International Journal of Vehicle Safety*, vol. 4, no. 1, pp. 45–83, 2009.
- [3] R. J. Anderson and E. F. Kurtz, "A critical assessment of the effects of a Trailer-Hitch load-transfer device on the handling characteristics of a car-trailer combination," in *The Dynamics of Vehicles on Roads*, Routledge, 2018, pp. 127–140.
- [4] R. Serban, M. Taylor, D. Negrut, and A. Tasora, "Chrono:Vehicle: template-based ground vehicle modelling and simulation," *International Journal of Vehicle Performance*, vol. 5, no. 1, p. 18, pp.18-39, 2019.
- [5] G. Moreno, L. C. Nicolazzi, R. D. S. Vieira, and D. Martins, "Stability of long combination vehicles," *International Journal of Heavy Vehicle Systems*, vol. 25, no. 1, pp. 113–131, 2018.
- [6] I. M. Zulhilmi, M. H. Peeie, R. I. M. Eiman, I. M. Izhar, and S. M. Asyraf, "Investigation on vehicle dynamic behaviour during emergency braking at different speed," *International Journal of Automotive and Mechanical Engineering*, vol. 16, no. 1, pp. 6161–6172, 2019.
- [7] I. O. for S. ISO, "Road vehicles — Mechanical couplings between tractors and semi-trailers — Part 3: Requirements for semi-trailer contact area to fifth wheel (ISO 1726-3:2010)," *International Organization for Standards Catalogue*, pp. 1–5, 2010.
- [8] T. Tudor and K. Tudor, "Analysis of Load Transfer with Respect to Non-Dynamic Steer Effects," United States: SAE International, No. 2016-01-0172, 2016.
- [9] M. Z. Abdul Manaf, K. Hudha, P. Mohd Samin, and S. A. Abu Bakar, "Modelling and verification of a 12-dof tractor-semitrailer longitudinal model for load transfer analysis," *International Journal of Heavy Vehicle Systems*, vol. 30, no. 5, pp. 525-559, 2023.
- [10] R. Nigam, "Characteristics of Fifth Wheel and its Influence on handling and maneuvering of Articulated Heavy vehicles," Chalmers University of Technology, 2018. [Online]. Available: <http://publications.lib.chalmers.se/records/fulltext/255452/255452.pdf>
- [11] A. Jogi and S. Chandramohan, "Kinematic analysis of tractor-semitrailer with split fifth wheel coupling during low speed turning maneuvers," *SAE International Journal of Commercial Vehicles*, vol. 10, no. 2, pp. 582–588, Mar. 2017.
- [12] F. L. Tagg and F. E. Tourville, "Fifth-wheel suspension system," U.S. Patent 4,279,430., 1981
- [13] J. D. Hume, "Stabilizer lever for tractor semitrailer fifth-wheel hitches," U.S. Patent 2,727,755., 1955
- [14] J. V Hendrickson and G. J. Hartwick, "Fifth wheel construction for force distribution between tractor and semitrailer," U.S. Patent 2,847,230., 1958
- [15] I. M. Ibrahim, "Design of a compensating fifth wheel for improving the roll dynamic behavior of the tractors semi-trailers," *SAE Technical Papers*, no. 724, 2002.
- [16] J. Han, "From PID to active disturbance rejection control," *IEEE Transactions on Industrial Electronics*, vol. 56, no. 3, pp. 900–906, 2009.
- [17] Y. Huang and W. Xue, "Active disturbance rejection control: Methodology and theoretical analysis," *ISA Transactions*, vol. 53, no. 4, pp. 963–976, 2014.
- [18] F. Hasbullah and W. F. Faris, "Simulation of disturbance rejection control of half-car active suspension system using active disturbance rejection control with decoupling transformation," *Journal of Physics: Conference Series*, vol. 949, no. 1, 2018.
- [19] R. Fareh, S. Khadraoui, M. Y. Abdallah, M. Baziyad, and M. Bettayeb, "Active disturbance rejection control for robotic systems: A review," *Mechatronics*, vol. 80, p. 102671, 2021.
- [20] F. Beltran-Carbajal, A. Valderrabano-Gonzalez, A. R. Favela-Contreras, and J. C. Rosas-Caro, "Active disturbance rejection control of a magnetic suspension system," *Asian Journal of Control*, vol. 17, no. 3, pp. 842–854, 2015.
- [21] G. Xu and N. Zhang, "Characteristic analysis of roll and pitch independently controlled hydraulically interconnected suspension," *SAE International Journal of Commercial Vehicles*, vol. 7, no. 1, pp. 170–176, 2014.
- [22] M. H. Harun, W. M. Z. W. Abdullah, H. Jamaluddin, R. A. Rahman, and K. Hudha, "Hybrid skyhook-stability augmentation system for ride quality improvement of railway vehicle," *Applied Mechanics and Materials*, vol. 663, pp. 141–145, 2014.
- [23] J. He, Y. Chen, C. Zhao, Z. Qi, and X. Ren, "Heavy truck suspension optimisation based on modified skyhook damping control," *International Journal of Heavy Vehicle Systems*, vol. 18, no. 2, p. 161, 2011.
- [24] G. Priyandoko, M. Mailah, and H. Jamaluddin, "Vehicle active suspension system using skyhook adaptive neuro active force control," *Mechanical Systems and Signal Processing*, vol. 23, no. 3, pp. 855–868, 2009.
- [25] M. H. I. M. Amin, K. Hudha, Z. A. Kadir, and N. H. Amer, "Skyhook control for 7 DOF ride model of armored vehicle due to road disturbance," *2015 10th Asian Control Conference: Emerging Control Techniques for a Sustainable World, ASCC 2015*, pp. 2–6, 2015.
- [26] K. Hudha, "Non-parametric modeling and modified hybrid skyhook groundhook control of magnetorheological dampers for automotive suspension system," PhD thesis, Universiti Teknologi Malaysia, Skudai, 2005.
- [27] L. Guo and S. Cao, "Anti-disturbance control theory for systems with multiple disturbances: A survey," *ISA Transactions*, vol. 53, no. 4, pp. 846–849, 2014.
- [28] S. K. Sharma, U. Saini, and A. Kumar, "Semi-active Control to Reduce Lateral Vibration of Passenger Rail Vehicle Using Disturbance Rejection and Continuous State Damper Controllers," *Journal of Vibration Engineering and Technologies*, vol. 7, no. 2, pp. 117–129, 2019.

- [29] K. Hudha, H. Jamaluddin, and P. Mohd Samin, "Disturbance rejection control of a light armoured vehicle using stability augmentation based active suspension system," *International Journal of Heavy Vehicle Systems*, vol. 15, no. 2/3/4, p. 152, 2008.
- [30] L. Z. Ben, F. Hasbullah, and F. W. Faris, "A comparative ride performance of passive, semi-active and active suspension systems for off-road vehicles using half car model," *International Journal of Heavy Vehicle Systems*, vol. 21, no. 1, p. 26, 2014.
- [31] F. Hasbullah, W. Faris, S. J. Darsivan and M. Abdelrahman, "Ride comfort performance of a non-linear full-car using active suspension system with active disturbance rejection control and input decoupling transformation," *International Journal of Heavy Vehicle Systems*, vol. 26, no. 2, pp. 188-224, 2019.
- [32] K. Pejhan, Q. Wang, C. Q. Wu, and I. Telichev, "Experimental validation of the U* index theory for load transfer analysis," *International Journal of Heavy Vehicle Systems*, vol. 24, no. 3, p. 288, 2017.
- [33] C. S. Díaz-Choque, L. C. Félix-Herrán, and R. A. Ramírez-Mendoza, "Optimal Skyhook and Groundhook Control for Semiactive Suspension: A Comprehensive Methodology," *Shock and Vibration*, vol. 2021, pp. 1–21, 2021.
- [34] C. Liu, L. Chen, X. Yang, X. Zhang, and Y. Yang, "General Theory of Skyhook Control and its Application to Semi-Active Suspension Control Strategy Design," *IEEE Access*, vol. 7, pp. 101552–101560, 2019.
- [35] X. Sun, Y. Cai, C. Yuan, L. Chen, and R. Wang, "Hybrid model predictive control of damping multi-mode switching damper for vehicle suspensions," *Journal of Vibroengineering*, vol. 19, no. 4, pp. 2910–2930, 2017.
- [36] P. J. Gawthrop, S. A. Neild, and D. J. Wagg, "Semi-active damping using a hybrid control approach," *Journal of Intelligent Material Systems and Structures*, vol. 23, no. 18, pp. 2103–2116, 2012.
- [37] P. Esnault and M. Klein, "Factors of safety and reliability," *Spacecraft Structures, Materials and Mechanical Engineering*, Roma, Italy: European Space Agency, pp. 109–119, 1996.
- [38] T. Xing and F. Stern, "Factors of Safety for Richardson Extrapolation," *Journal of Fluids Engineering*, vol. 132, no. 6, pp. 0614031–0640313, 2010.
- [39] P. R. N. Childs, "Fastening and Power Screws," *Mechanical Design*, Elsevier, pp. 371–412, 2021.
- [40] C. G. Zhou, H. T. Feng, and Y. Ou, "A new model for predicting the mechanical efficiency of ball screws based on the empirical equations for the friction torque of rolling bearings," *Advances in Mechanical Engineering*, vol. 10, no. 9, pp. 1–8, 2018.
- [41] N. H. Amer, H. Zamzuri, K. Hudha, V. R. Aparow, Z. A. Kadir, and A. F. Z. Abidin, "Path tracking controller of an autonomous armoured vehicle using modified Stanley controller optimized with particle swarm optimization," *Journal of the Brazilian Society of Mechanical Sciences and Engineering*, vol. 40, no. 2, p. 104, 2018.
- [42] N. H. Amer, K. Hudha, H. Zamzuri, V. R. Aparow, Z. A. Kadir, and A. F. Zainal Abidin, "Hardware-in-the-loop simulation of trajectory following control for a light armoured vehicle optimised with particle swarm optimisation," *International Journal of Heavy Vehicle Systems*, vol. 26, no. 5, pp. 663–691, 2019.
- [43] M. H. I. M. Amin, K. Hudha, N. H. Amer, Z. A. Kadir, and A. Faiz, "Modelling and Control of Seven Dof Ride Model Using Hybrid Controller Optimized by Particle Swarm Optimization," *Journal of Engineering and Technology*, vol. 6, no. 2, pp. 121–142, 2015.
- [44] S. Thanok and M. Parnichkun, "Longitudinal control of an intelligent vehicle using particle swarm optimization based sliding mode control," *Advanced Robotics*, vol. 29, no. 8, pp. 525–543, 2015.
- [45] R. R. Mutra and J. Srinivas, "An Integrated Bearing Parameter Identification Approach Using A Nonlinear Optimisation Scheme," *International Journal of Automotive and Mechanical Engineering*, vol. 16, no. 1, pp. 6245–6262, 2019.
- [46] Meenu and S. Kumar, "Optimization of the Material Removal Rate in Turning of UD-GFRP using the Particle Swarm Optimization Technique," *International Journal of Automotive and Mechanical Engineering*, vol. 8, no. 1, pp. 1226–1241, 2013.
- [47] X. Kang, S. Rakheja, and I. Stiharu, "Cargo load shift and its influence on tank vehicle dynamics under braking and turning," *International Journal of Heavy Vehicle Systems*, vol. 9, no. 3, p. 173, 2002.
- [48] J. Jabatan Pengangkutan Jalan Malaysia, "Current Situation of Heavy Vehicle Overloading in Malaysia," *Workshop on Regulating High Mass Heavy Road Vehicles for Safety, Productivity and Infrastructure Outcomes*, Brisbane, Australia: Asia-Pacific Economic Cooperation, pp. 1–20, 2017.
- [49] M. K. Salaani, P. A. Grygier, and G. J. Heydinger, "Evaluation of Heavy Tractor-Trailer Model used in the National Advanced Driving Simulator," *2003 SAE World Congress*, Detroit, Michigan: SAE International, 2003.
- [50] A. Goodarzi, J. Mehrmashhadi, and E. Esmailzadeh, "Optimised braking force distribution strategies for straight and curved braking," *International Journal of Heavy Vehicle Systems*, vol. 16, no. 1–2, pp. 78-101, 2009.
- [51] W. J. Evers, I. Besselink, H. Nijmeijer, and A. Van der Knaap, "Development and validation of a modular simulation model for commercial vehicles," *International Journal of Heavy Vehicle Systems*, vol. 16, no. 1/2, p. 132, 2009.
- [52] W. Huang, Y. Fan, and M. Yu, "Research on loaded brake performance test of trucks," *International Journal of Heavy Vehicle Systems*, vol. 27, no. 5, p. 648, 2020.
- [53] F. Ahmad, S. A. Mazlan, H. Zamzuri, H. Jamaluddin, K. Hudha, and M. Short, "Modelling and validation of the vehicle longitudinal model," *International Journal of Automotive and Mechanical Engineering*, vol. 10, no. 1, pp. 2042–2056, 2014.
- [54] A. Z. Zainordin, Z. Mohamed, and F. Ahmad, "Magnetorheological Fluid: Testing on Automotive Braking System," *International Journal of Automotive and Mechanical Engineering*, vol. 18, no. 1, pp. 8577–8584, 2021.
- [55] E. Kutluay and H. Winner, "Validation of vehicle dynamics simulation models - A review," *Vehicle System Dynamics*, vol. 52, no. 2, pp. 186–200, 2014.

- [56] V. R. Aparow, K. Hudha, M. M. H. Megat Ahmad, and H. Jamaluddin, “Development and verification of a 9-DOF armored vehicle model in the lateral and longitudinal directions,” *Jurnal Teknologi*, vol. 6, pp. 117–137, 2016.
- [57] K. Hudha, Z. A. Kadir, M. R. Said, and H. Jamaluddin, “Modelling, validation and roll moment rejection control of pneumatically actuated active roll control for improving vehicle lateral dynamics performance,” *International Journal of Engineering Systems Modelling and Simulation*, vol. 1, no. 2–3, pp. 122–136, 2009.
- [58] M. Hafiz Harun, P. M. Samin, K. Hudha, S. A. A. Bakar, and A. M. Saad, “Modelling and verification of tractor ride model,” *IOP Conference Series: Materials Science and Engineering*, vol. 469, no. 1, pp. 1–10, 2019.
- [59] P. M. Samin, H. Jamaluddin, R. A. Rahman, S. Anuar, A. Bakar, and K. Hudha, “Semi-active suspension for ride improvement using stability augmentation system control algorithm,” *Jurnal Mekanikal*, no. 26, pp. 86–95, 2008.
- [60] S. A. A. Bakar *et al.*, “Active suspension system in improving ride and handling performance of electric vehicle conversion,” *International Journal of Electric and Hybrid Vehicles*, vol. 4, no. 1, pp. 24–53, 2012.

NOMENCLATURE

M_{pr}	pitch rate moment [Nm]
M_{pmr}	pitch moment rejection [Nm]
M_{sky}	Skyhook moment [Nm]
$M_{a,des}$	desired actuator moment [Nm]
M_{pc}	pitch moment at semitrailer’s pitch centre [Nm]
$F_{a,des}$	desired actuator force [N]
F_a	actuator force [N]
F_{ps}	power-screw force [N]
T_{ps}	power-screw torque [Nm]
$T_{pslift/lower}$	power-screw torque to raise or lower the DHIL actuator [Nm]
P_{motor}	power-screw/electric motor power [W]
$\dot{\theta}_{ref}$	reference pitch rate [deg/s]
$\dot{\theta}_{real}$	actual pitch rate [deg/s]
ω_{ps}	power-screw/electric motor angular velocity [rad/s]
n_{sp}	power-screw/electric motor speed [rev/s]
$e_1(t)$	pitch rate error [deg/s]
K_{p1}	PID controller parameter – proportional gain for loop 1
K_{i1}	PID controller parameter – integral gain for loop 1
K_{d1}	PID controller parameter – derivative gain for loop 1
K_{p4}	PID controller parameter – proportional gain for loop 4
C_{sky}	Skyhook moment gain [Nm.s/deg]
K_1	pitch moment rejection gain/load transfer uncertainty gain for tractor
K_2	pitch moment rejection gain/load transfer uncertainty gain for semitrailer
LT_{ref}	load transfer reference from the passive vehicle [N]
LT_{model}	actual load transfer from the active vehicle [N]
m_1	tractor sprung mass [kg]
m_2	semitrailer sprung mass [kg]
a_x	longitudinal acceleration [m/s ²]
d	semitrailer pitchpole [m]
H	tractor CG height [m]
H_1	hitch height from the ground [m]
H_2	semitrailer CG height [m]
H_3	DHIL actuator hitch table vertical displacement/lift height [m]

NOMENCLATURE

C_1	distance from tractor CG to the tractor front axle [m]
C_2	distance from semitrailer CG to the hitch joint [m]
B_1	distance from tractor CG to the tractor rear axle [m]
B_2	distance from semitrailer CG to the semitrailer rear axle [m]

Q	DHIL actuator long arm length [m]
P	DHIL actuator short arm length [m]
α	power-screw thread angle (for ACME, $2\alpha = 29^\circ$)
β	the angle between the DHIL actuator short arm and base [degree]
d_s	screw means (pitch) diameter [m]
d_c	collar diameter [m]
μ_s	screw friction
μ_c	collar friction
l_s	power-screw lead/pitch (for multiple pitch = $m \cdot l_s$, m = number of pitches)